

ANALYSIS AND NUMERICAL SOLVER FOR EXCITATORY-INHIBITORY NETWORKS WITH DELAY AND REFRACTORY PERIODS

MARÍA J. CÁCERES* AND RICARDA SCHNEIDER

Abstract. The network of noisy leaky integrate and fire (NNLIF) model is one of the simplest self-contained mean-field models considered to describe the behavior of neural networks. Even so, in studying its mathematical properties some simplifications are required [Cáceres and Perthame, *J. Theor. Biol.* **350** (2014) 81–89; Cáceres and Schneider, *Kinet. Relat. Model.* **10** (2017) 587–612; Cáceres, Carrillo and Perthame, *J. Math. Neurosci.* **1** (2011) 7] which disregard crucial phenomena. In this work we deal with the general NNLIF model without simplifications. It involves a network with two populations (excitatory and inhibitory), with transmission delays between the neurons and where the neurons remain in a refractory state for a certain time. In this paper we study the number of steady states in terms of the model parameters, the long time behaviour *via* the entropy method and Poincaré’s inequality, blow-up phenomena, and the importance of transmission delays between excitatory neurons to prevent blow-up and to give rise to synchronous solutions. Besides analytical results, we present a numerical solver, based on high order flux-splitting WENO schemes and an explicit third order TVD Runge-Kutta method, in order to describe the wide range of phenomena exhibited by the network: blow-up, asynchronous/synchronous solutions and instability/stability of the steady states. The solver also allows us to observe the time evolution of the firing rates, refractory states and the probability distributions of the excitatory and inhibitory populations.

Mathematics Subject Classification. 35K60, 35Q92, 82C31, 82C32, 92B20

Received June 9, 2017. Accepted February 13, 2018.

1. INTRODUCTION

Neuroscience uses a wide variety of models based on ordinary differential equations (ODEs) and/or partial differential equations (PDEs). In recent years, analytical and numerical research shed light in the study of their mathematical properties. There is a large number of microscopic models consisting of systems of Stochastic differential equations (SDEs), where each equation describes the behavior of one of the network’s neurons. There are many works that perform numerical simulations for these microscopic models using the Monte-Carlo method [14, 15, 49, 50, 58, 60, 61, 66]. However, from a computational point of view, it is complicated to deal with networks with a large number of neurons. Mean-field models overcome this difficulty, since they determine the evolution of the network through density functions that are solutions of one (or a few) PDEs.

Keywords and phrases: Neural networks, Leaky integrate and fire models, noise, blow-up, steady states, entropy; long time behavior, refractory states, transmission delay.

Departamento de Matemática Aplicada, Campus de Fuentenueva, Universidad de Granada, 18071 Granada, Spain.

* Corresponding author: caceresg@ugr.es

This procedure is applied, *e.g.*, in [5, 21, 33, 34, 39, 43, 51, 52, 76, 80]. Usually, these models permit to recover macroscopic quantities as, *e.g.*, the global firing rate of the network, which can be compared with the corresponding macroscopic quantities of the SDEs.

In this paper, we study the network of noisy leaky integrate and fire neuron (NNLIF) system from an analytical and a numerical point of view. It is one of the simplest self-contained mean-field models considered for the description of neural networks. It was initially presented in [7] and is based on a nonlinear system of two PDEs of Fokker-Planck type and two ODEs. All the equations are nonlinearly coupled, and some terms are time-delayed. The system represents the behaviour of a network with excitatory and inhibitory neurons, considered as different populations, and described at a microscopic level by the leaky IF model. Their unknowns are $\rho_\alpha(t, v)$ and $R_\alpha(t)$. The probability densities $\rho_\alpha(t, v)$ describe the limiting probability of a neuron of the excitatory population ($\alpha = E$) or of the inhibitory one ($\alpha = I$), with a membrane potential v at time t , when the total number of neurons of the network, n , goes to infinity. And the refractory states $R_\alpha(t)$, one for each population, represent the limiting proportion of neurons that do not respond to stimuli.

To achieve a better understanding of the mathematical properties of the model, some crucial phenomena were disregarded in the literature. For example, the transmission delay of the neural spike, the existence of refractory states, or the fact that there are two populations [10–12]. The simplest NNLIF model, widely studied in [12, 19, 20], corresponds to the case in which the neural network is assumed to be composed of only one population, which can be average-excitatory or average-inhibitory, and where the neurons always respond to stimuli. Mathematically it means that there is a PDE, with a *connectivity parameter* b , whose sign determines whether the population is average-excitatory (positive b) or average-inhibitory (negative b). The inclusion of the refractory state was analyzed in [10, 11] investigated a model for two populations without delays and without refractory states. Some other works have studied IF neural networks at microscopic level through stochastic equations. Among them we point out [24, 25]. Moreover, [7, 10–12, 19, 20, 24, 25] provide complementary results at different levels of description. As a matter of fact, they can be considered as the starting point of the research of this paper, as we explain later on.

The aim of the current work is to study mathematical aspects of a more realistic NNLIF model consisting of two populations with refractory states and transmission delays. We demonstrate that neural networks with part of their neurons in a refractory state always have steady states. Therefore, the presence of refractory states produces at least one steady state, while in the absence of refractory periods [11] there are some values of the parameters for which the model has no steady states. We are also able to give conditions for the values of the model parameters which ensure the uniqueness of the steady state. This result is completed with a proof of exponential convergence of the solution to the steady state for networks with small connectivity parameters and without transmission delay. The entropy method [11, 20] will be used to achieve this goal, with the additional difficulty that we deal with a complex system involving four equations, for which the entropy functional is composed of excitatory and inhibitory densities and their corresponding refractory probabilities. These results were already known for the simpler case of only one population [10, 12].

Moreover, we extend to this case the analysis of blow-up phenomena started in [10, 11] for this Fokker-Planck model. We will observe that the network can blow-up in finite time if the transmission delay between excitatory neurons vanishes, even if there are transmission delays between inhibitory neurons or between inhibitory and excitatory neurons. Consequently, we show that the only way to avoid the blow-up is to consider a nonzero transmission delay between excitatory neurons. At the microscopic level, it is known that global-in-time solutions exist under the presence of transmission delays in the case of only one average-excitatory population (see [24, 25]). In that direction, in [27] it was shown that the blow-up disappears also for the Omurtag-Dumont model if there is a nonzero delay. This model, which was initially presented in [53], is closely related to the NNLIF one, since it appears from the same microscopic approximation as the NNLIF model. Thus, its unknown ρ refers to a similar probability density. Concerning the explosion, we refer to [35, 64], for a discussion about the suitability of the random IF models. Furthermore, there is a great deal of works that include the delay in neural models. For instance [73–75], where it is taken into account the spatial distribution of the populations, too.

Some analytical problems related to this model remain open. In order to better understand them and to visually show the behaviour of the network, we develop a numerical solver for the full model. Our solver is based

on high order flux-splitting weighted essentially non oscillatory (WENO) schemes, total variation diminishing (TVD) Runge-Kutta methods, and an efficient numerical strategy to deal with the saving and recovering of data needed to take the delays into account. This new numerical solver improves our previous ones [10–12] not only because it describes the complete NNLIIF model, but also because it has been optimized. It allows us to describe the wide range of phenomena displayed by the network: blow-up, asynchronous/synchronous solutions, instability/stability of the steady states, as well as the time evolution of the firing rates, the proportion of refractory states, and the probability distributions of the excitatory and inhibitory populations. Besides, we numerically explore the importance of the transmission delay between excitatory neurons to avoid the blow-up phenomenon. Blow-up without delay is prevented if a nonzero transmission delay is considered. Instead of blowing-up, solutions approach a stationary solution, a *synchronous state*, or the firing rates increase without blowing-up in finite time. Notice that the appearance of oscillatory solutions in neural networks is a known fact, that has been widely studied in, *e.g.*, [1, 7–9, 49, 50, 55, 61]. To our knowledge, the numerical solver presented in this paper is the first deterministic solver to describe the behavior of the full NNLIIF system including all the characteristic phenomena of real networks. Other deterministic solvers for related neural PDE models can be found, for instance [4, 13, 50, 51, 55, 56, 58].

Developing efficient numerical solvers that consider all relevant phenomena is essential to work out strategies that, on the one hand, give answer to the open questions as for instance the stability in the case of large connectivity parameters, the importance of the transmission delay to avoid the blow-up of the solutions and to produce periodic solutions, or the study of conditions for which synchronous solutions appear; and, on the other hand, help to implement solvers for other large-scaled models, which are becoming more common in computational neuroscience [41, 46, 59, 69, 70, 77].

Our work is related to the results presented in [7] and we expect to complete them in two directions: On one hand, our numerical scheme reproduces situations studied in [7] and provides the time evolution of the firing rates, the refractory states and the probability distributions, and, on the other hand, we contribute to the analytical study of the number of steady states, their stability for small connectivity parameters, the blow-up phenomenon and the importance of the transmission delay to avoid it.

There are many other PDE models that are used to describe the behavior of neural networks: Population density models of IF neurons with jumps [26–28, 53], Fokker-Planck equations for uncoupled neurons [49, 50]; Fokker-Planck equations including conductance variables, [13, 57, 61] (and references therein), time elapsed models [54–56] which have been recently derived as mean-field limits of Hawkes processes [22, 23], McKean-Vlasov equations [2, 48], which are the mean-field equations related to the behaviour of Fitzhugh-Nagumo neurons [32], etc. Finding relations between these different families of PDEs is an interesting issue. The works [29–31] are in that direction, since the authors showed connections between some Fokker-Planck equations and the elapsed models.

The paper is structured as follows. In the second section we describe the model and the concept of solution considered. In Section 3 we analyze the number of steady states, prove exponential convergence to the unique stationary solution when the connectivity parameters are small enough, and present a criterion to obtain solutions that blow-up in finite time. Our numerical scheme is detailed in Section 4. In Section 5 we illustrate the theoretical results and explore the complex dynamics of the NNLIIF model in some aspects that have not been treated from an analytical point of view due to its complexity. Finally, in Section 6 we present some conclusions and open problems.

2. THE MODEL

In this section we provide the conceptual mathematical and biological framework of this paper. We explain how the system of PDEs and ODEs, that represents the full NNLIIF model, is derived from the biological model that describes the behavior of the neurons at a microscopic level, by means of IF neuron models. We refer to [6–8, 28, 35, 36, 38, 62, 64, 65, 71, 72, 78], and references therein, for a background on different versions of the IF model and its validation as a suitable neuroscience model.

We consider a neural network with n neurons (n_E excitatory and n_I inhibitory) described by the IF model, which depicts the activity of the membrane potential. The time evolution of the membrane potential $V_\alpha(t)$ of an inhibitory neuron ($\alpha = I$) or an excitatory one ($\alpha = E$) is given by the following equation (see [7, 8] for details)

$$C_m \frac{dV^\alpha}{dt}(t) = -g_L(V^\alpha(t) - V_L) + I^\alpha(t), \tag{2.1}$$

where C_m is the capacitance of the membrane, g_L is the leak conductance, V_L is the leak reversal potential and $I^\alpha(t)$ is the incoming synaptic current, which models all the interactions of the neuron with other neurons. In the absence of interactions with other neurons ($I^\alpha(t) = 0$), the membrane potential relaxes towards a resting value V_L . However, the interaction with other neurons provokes the neuron to fire, that is, it emits an action potential (spike) when $V^\alpha(t)$ reaches its threshold or firing value V_F , and the membrane potential relaxes to a reset value V_R . (Let us remark that $V_L < V_R < V_F$). Each neuron receives C_{ext} connections from excitatory neurons outside the network and $C = C_E + C_I$ connections from neurons in the network, of which $C_E = \epsilon n_E$ are from excitatory neurons and $C_I = \epsilon n_I$ are from inhibitory neurons. These connections are assumed to be randomly chosen, and the network to be sparsely connected, namely, $\epsilon = \frac{C_E}{n_E} = \frac{C_I}{n_I} \ll 1$, see [7]. The synaptic current $I^\alpha(t)$ takes the form of the following stochastic process

$$I^\alpha(t) = J_E^\alpha \sum_{i=1}^{\bar{C}_E} \sum_j \delta(t - t_{Ej}^i - D_E^\alpha) - J_I^\alpha \sum_{i=1}^{C_I} \sum_j \delta(t - t_{Ij}^i - D_I^\alpha), \quad \alpha = E, I,$$

where $D_E^\alpha \geq 0$, $D_I^\alpha \geq 0$ are the synaptic delays, t_{Ej}^i and t_{Ij}^i are the times of the j th-spike coming from the i th-presynaptic neuron for excitatory and inhibitory neurons, respectively, $\bar{C}_E = C_E + C_{\text{ext}}$, and J_k^α , for $\alpha, k = E, I$, are the strengths of the synapses. The stochastic character is enclosed in the distribution of the spike times of the neurons. The spike trains of all neurons in the network are supposed to be described by Poisson processes with a common instantaneous firing rate, $\nu_\alpha(t)$, $\alpha = E, I$. These processes are supposed to be independent [7, 12]. By using these hypotheses and assuming $C_{\text{ext}} = C_E$, the mean value of the current, $\mu_C^\alpha(t)$, and its variance, $\sigma_C^{\alpha 2}(t)$, take the form

$$\mu_C^\alpha(t) = C_E J_E^\alpha \nu_E(t - D_E^\alpha) - C_I J_I^\alpha \nu_I(t - D_I^\alpha), \tag{2.2}$$

$$\sigma_C^{\alpha 2}(t) = C_E (J_E^\alpha)^2 \nu_E(t - D_E^\alpha) + C_I (J_I^\alpha)^2 \nu_I(t - D_I^\alpha). \tag{2.3}$$

Many authors [7, 8, 47, 53] approximate the incoming synaptic current by a continuous-in-time stochastic process of Ornstein-Uhlenbeck type which has the same mean and variance as the Poissonian spike-train process. Specifically, $I^\alpha(t)$ is approached by

$$I^\alpha(t)dt \approx \mu_C^\alpha(t) dt + \sigma_C^\alpha(t) dB_t, \quad \alpha = E, I, \tag{2.4}$$

where B_t is the standard Brownian motion. This diffusion approximation becomes exact in the infinitely large network limit, $n \rightarrow \infty$, if the synaptic strengths J_E^α and J_I^α , $\alpha = E, I$, are scaled appropriately with the network sizes C_E and C_I , as shown in [62].

Summing up, the approximation to the stochastic differential model (2.1), taking the voltage and time units so that $C_m = g_L = 1$, finally yields

$$dV^\alpha(t) = (-V^\alpha(t) + V_L + \mu_C^\alpha(t)) dt + \sigma_C^\alpha(t) dB_t, \quad V^\alpha \leq V_F, \quad \alpha = E, I, \tag{2.5}$$

with the jump process $V^\alpha(t_0^+) = V_R$, $V^\alpha(t_0^-) = V_F$, whenever at t_0 the voltage reaches the threshold value V_F . The firing rate or probability of firing per unit time of the Poissonian spike train, $\nu_\alpha(t)$, is calculated in [62] as

$$\nu_\alpha(t) = \nu_{\alpha,\text{ext}} + N_\alpha(t), \quad \alpha = E, I,$$

where $\nu_{\alpha,\text{ext}}$ is the frequency of the external input and $N_\alpha(t)$ is the mean firing rate of the population α . Also, $\nu_{I,\text{ext}} = 0$ since the external connections are with excitatory neurons.

Going back to (2.5), a system of coupled PDEs for the evolution of the probability densities $\rho_\alpha(v, t)$ can be written, where $\rho_\alpha(v, t)$ denotes the limiting probability of finding a neuron in the population α , with a voltage $v \in (-\infty, V_F]$ at a time $t \geq 0$.

Using Itô's rule [7, 8, 47, 53, 63], the stochastic equations (2.1) and (2.4) are transformed into a system of coupled Fokker-Planck or backward Kolmogorov equations with sources

$$\begin{cases} \frac{\partial \rho_I}{\partial t}(v, t) + \frac{\partial}{\partial v} [h^I(v, N_E(t - D_E^I), N_I(t - D_I^I)) \rho_I(v, t)] - a_I(N_E(t - D_E^I), N_I(t - D_I^I)) \frac{\partial^2 \rho_I}{\partial v^2}(v, t) \\ = M_I(t) \delta(v - V_R), \\ \frac{\partial \rho_E}{\partial t}(v, t) + \frac{\partial}{\partial v} [h^E(v, N_E(t - D_E^E), N_I(t - D_I^E)) \rho_E(v, t)] - a_E(N_E(t - D_E^E), N_I(t - D_I^E)) \frac{\partial^2 \rho_E}{\partial v^2}(v, t) \\ = M_E(t) \delta(v - V_R), \end{cases} \quad (2.6)$$

with $h^\alpha(v, N_E(t - D_E^\alpha), N_I(t - D_I^\alpha)) = -v + V_L + \mu_C^\alpha$ and $a_\alpha(N_E(t - D_E^\alpha), N_I(t - D_I^\alpha)) = \frac{\sigma_C^{\alpha 2}}{2}$. The right hand sides in (2.6) represent the fact that when neurons reach the threshold potential V_F , they emit a spike over the network, reset their membrane potential to the reset value V_R and remain some time in a refractory period, denoted τ_α . Different choices of $M_\alpha(t)$ can be considered: $M_\alpha(t) = N_\alpha(t - \tau_\alpha)$, as studied in [7], or $M_\alpha(t) = \frac{R_\alpha(t)}{\tau_\alpha}$, as proposed in [10]. Thus, system (2.6) is completed with two ODEs for $R_\alpha(t)$, the limiting probabilities to find a neuron from population α in the refractory state,

$$\frac{dR_\alpha(t)}{dt} = N_\alpha(t) - M_\alpha(t), \quad \forall \alpha = E, I, \quad (2.7)$$

Dirichlet boundary conditions and initial data

$$\rho_\alpha(-\infty, t) = 0, \quad \rho_\alpha(V_F, t) = 0, \quad \rho_\alpha(v, 0) = \rho_\alpha^0(v) \geq 0, \quad R_\alpha(0) = R_\alpha^0 \geq 0, \quad \alpha = E, I. \quad (2.8)$$

In order to simplify the notation, we denote $d_k^\alpha = C_k(J_k^\alpha)^2 \geq 0$ and $b_k^\alpha = C_k J_k^\alpha \geq 0$ for $k, \alpha = E, I$, and the variable v is translated with the factor $V_L + b_E^E \nu_{E,\text{ext}}$. Let us remark that we keep the same notation for the other involved values (V_R , V_F) and also v for the new variable. With the new voltage variable and using expressions (2.2) and (2.3) for $\mu_C^\alpha(t)$ and $\sigma_C^\alpha(t)$, the drift and diffusion coefficients become

$$h^\alpha(v, N_E(t - D_E^\alpha), N_I(t - D_I^\alpha)) = -v + b_E^\alpha N_E(t - D_E^\alpha) - b_I^\alpha N_I(t - D_I^\alpha) + (b_E^\alpha - b_E^E) \nu_{E,\text{ext}}, \quad (2.9)$$

$$a_\alpha(N_E(t - D_E^\alpha), N_I(t - D_I^\alpha)) = d_E^\alpha \nu_{E,\text{ext}} + d_E^\alpha N_E(t - D_E^\alpha) + d_I^\alpha N_I(t - D_I^\alpha), \quad \alpha = E, I. \quad (2.10)$$

The coupling of the system (2.6) is hidden in these two terms, since the mean firing rates N_α obey to

$$N_\alpha(t) = -a_\alpha(N_E(t), N_I(t)) \frac{\partial \rho_\alpha}{\partial v}(V_F, t) \geq 0, \quad \alpha = E, I. \quad (2.11)$$

Moreover, (2.11) gives rise to the nonlinearity of (2.6), since firing rates are defined in terms of boundary conditions on the distribution functions ρ_α . On the other hand, since R_E and R_I represent probabilities and

ρ_E and ρ_I are probability densities, the total mass is conserved:

$$\int_{-\infty}^{V_F} \rho_\alpha(v, t) \, dv + R_\alpha(t) = \int_{-\infty}^{V_F} \rho_\alpha^0(v) \, dv + R_\alpha^0 = 1 \quad \forall t \geq 0, \quad \alpha = E, I. \tag{2.12}$$

To finish the description of the model, we remark that system (2.6) also includes the case of only one population (in average excitatory or inhibitory), with refractory state and transmission delay. Specifically, we can remove α in (2.6) by considering only one PDE for the probability density, $\rho(v, t)$, which is coupled to an ODE for the probability that a neuron is in a refractory state, $R(t)$:

$$\begin{cases} \frac{\partial \rho}{\partial t}(v, t) + \frac{\partial}{\partial v}[h(v, N(t - D))\rho(v, t)] - a(N(t - D))\frac{\partial^2 \rho}{\partial v^2}(v, t) = M(t)\delta(v - V_R), \\ \frac{dR(t)}{dt} = N(t) - M(t), \quad \text{with } M(t) = N(t - \tau) \quad \text{or } M(t) = R(t)/\tau, \\ N(t) = -a(N(t - D))\frac{\partial \rho}{\partial v}(V_F, t) \geq 0, \\ \rho(-\infty, t) = 0, \quad \rho(V_F, t) = 0, \quad \rho(v, 0) = \rho^0(v) \geq 0, \quad R(0) = R^0, \end{cases} \tag{2.13}$$

with drift and diffusion terms

$$h(v, N(t)) = -v + bN(t) + \nu_{\text{ext}}, \tag{2.14}$$

$$a(N(t)) = d_0 + d_1N(t), \tag{2.15}$$

where the connectivity parameter b is positive for an average-excitatory population and negative for an average-inhibitory population, $d_0 > 0$, $d_1 \geq 0$, $\tau > 0$ is the refractory period, and ν_{ext} describes the external firing rate (note that this parameter and $\nu_{E,\text{ext}}$ have different units, since ν_{ext} includes other model constants).

To conclude the presentation of the model, we introduce the notion of solution that we consider in this work (see [10–12]).

Definition 2.1. Let $\rho_\alpha \in L^\infty(\mathbb{R}^+; L^1_+((-\infty, V_F)))$, $N_\alpha \in L^1_{loc,+}(\mathbb{R}^+)$ and $R_\alpha \in L^\infty_+(\mathbb{R}^+)$ for $\alpha = E, I$. Then $(\rho_E, \rho_I, R_E, R_I, N_E, N_I)$ is a weak solution of (2.6)–(2.10) if for any test function $\phi(v, t) \in C^\infty((-\infty, V_F] \times [0, T])$ and such that $\frac{\partial^2 \phi}{\partial v^2}, v \frac{\partial \phi}{\partial v} \in L^\infty((-\infty, V_F) \times (0, T))$, the following relation

$$\begin{aligned} & \int_0^T \int_{-\infty}^{V_F} \rho_\alpha(v, t) \left[-\frac{\partial \phi}{\partial t} - \frac{\partial \phi}{\partial v} h^\alpha(v, N_E(t - D_E^\alpha), N_I(t - D_I^\alpha)) - a_\alpha(N_E(t - D_E^\alpha), N_I(t - D_I^\alpha)) \frac{\partial^2 \phi}{\partial v^2} \right] \, dv \, dt \\ & = \int_0^T [M_\alpha(t)\phi(V_R, t) - N_\alpha(t)\phi(V_F, t)] \, dt + \int_{-\infty}^{V_F} \rho_\alpha^0(v)\phi(v, 0) \, dv - \int_{-\infty}^{V_F} \rho_\alpha(v, T)\phi(v, T) \, dv \end{aligned} \tag{2.16}$$

is satisfied, and R_α are solutions of the ODEs

$$\frac{dR_\alpha(t)}{dt} = N_\alpha(t) - M_\alpha(t).$$

We recall some notations involved in Definition 2.1. For $1 \leq p < \infty$, $L^p(\Omega)$ is the space of functions such that f^p is integrable in Ω , $L^\infty(\Omega)$ is the space of essentially bounded functions in Ω , $L^\infty_+(\Omega)$ represents the space of non-negative essentially bounded functions in Ω , $C^\infty(\Omega)$ is the set of infinitely differentiable functions in Ω , and $L^1_{loc,+}(\Omega)$ denotes the set of non-negative functions that are locally integrable in Ω .

3. STEADY STATES AND LONG TIME BEHAVIOR

The study of the number of steady states for excitatory and inhibitory NNLIF neural networks, with refractory periods and transmission delays of the spikes (2.6) (considering R_α either as defined in [10] or in [7]), can be done combining the ideas of [10–12], with the additional difficulty that the system to be dealt with is now more complicated, because there are two coupled non-linear PDEs and two ODEs. The steady states $(\rho_E, \rho_I, N_E, N_I, R_E, R_I)$ of (2.6) satisfy

$$\frac{\partial}{\partial v} [h^\alpha(v)\rho_\alpha(v) - a_\alpha(N_E, N_I)\frac{\partial \rho_\alpha}{\partial v}(v) + \frac{R_\alpha}{\tau_\alpha}H(v - V_R)] = 0, \quad R_\alpha = \tau_\alpha N_\alpha, \quad \alpha = E, I,$$

in the sense of distributions, with H denoting the Heaviside function and $h^\alpha(v, N_E, N_I) = V_0^\alpha(N_E, N_I) - v$, where $V_0^\alpha(N_E, N_I) = b_E^\alpha N_E - b_I^\alpha N_I + (b_E^\alpha - b_E^E)\nu_{E,\text{ext}}$. We remark that this equation is the same as the equation for stationary solutions in a network without transmission delays. Using the definition of N_α and the Dirichlet boundary conditions of (2.6) we obtain an initial value problem for every $\alpha = E, I$, whose solutions are

$$\rho_\alpha(v) = \frac{N_\alpha}{a_\alpha(N_E, N_I)} e^{-\frac{(v - V_0^\alpha(N_E, N_I))^2}{2a_\alpha(N_E, N_I)}} \int_{\max(v, V_R)}^{V_F} e^{-\frac{(w - V_0^\alpha(N_E, N_I))^2}{2a_\alpha(N_E, N_I)}} dw \quad \alpha = E, I. \tag{3.1}$$

Moreover, the conservation of mass (2.12), which takes into account the refractory states, yields a system of implicit equations for N_α

$$1 - \tau_\alpha N_\alpha = \frac{N_\alpha}{a_\alpha(N_E, N_I)} \int_{-\infty}^{V_F} e^{-\frac{(v - V_0^\alpha(N_E, N_I))^2}{2a_\alpha(N_E, N_I)}} \int_{\max(v, V_R)}^{V_F} e^{-\frac{(w - V_0^\alpha(N_E, N_I))^2}{2a_\alpha(N_E, N_I)}} dw dv. \tag{3.2}$$

If this system could be solved, the profile (3.1) would provide an exact expression for ρ_α . In order to handle the previous system more easily, we use two changes of variables as in [11]. First:

$$\begin{aligned} z &= \frac{v - V_0^E(N_E, N_I)}{\sqrt{a_E(N_E, N_I)}}, \quad u = \frac{w - V_0^E(N_E, N_I)}{\sqrt{a_E(N_E, N_I)}}, \quad w_F := \frac{V_F - V_0^E(N_E, N_I)}{\sqrt{a_E(N_E, N_I)}}, \quad w_R := \frac{V_R - V_0^E(N_E, N_I)}{\sqrt{a_E(N_E, N_I)}}, \\ \tilde{z} &= \frac{v - V_0^I(N_E, N_I)}{\sqrt{a_I(N_E, N_I)}}, \quad \tilde{u} = \frac{w - V_0^I(N_E, N_I)}{\sqrt{a_I(N_E, N_I)}}, \quad \tilde{w}_F := \frac{V_F - V_0^I(N_E, N_I)}{\sqrt{a_I(N_E, N_I)}}, \quad \tilde{w}_R := \frac{V_R - V_0^I(N_E, N_I)}{\sqrt{a_I(N_E, N_I)}}, \end{aligned}$$

and (3.2) is then written as

$$\begin{aligned} \frac{1}{N_E} - \tau_E &= I_1(N_E, N_I), \quad \text{where } I_1(N_E, N_I) = \int_{-\infty}^{w_F} e^{-\frac{z^2}{2}} \int_{\max(z, w_R)}^{w_F} e^{-\frac{u^2}{2}} du dz, \\ \frac{1}{N_I} - \tau_I &= I_2(N_E, N_I), \quad \text{where } I_2(N_E, N_I) = \int_{-\infty}^{\tilde{w}_F} e^{-\frac{\tilde{z}^2}{2}} \int_{\max(\tilde{z}, \tilde{w}_R)}^{\tilde{w}_F} e^{-\frac{\tilde{u}^2}{2}} d\tilde{u} d\tilde{z}. \end{aligned} \tag{3.3}$$

As a consequence of (3.3), and the positivity of I_1 and I_2 , we observe that the stationay firing rates satisfy:

$$N_\alpha < \frac{1}{\tau_\alpha} \quad \alpha = E, I. \tag{3.4}$$

And therefore, $R_\alpha = \tau_\alpha N_\alpha < 1$. Next, the change of variables $s = \frac{z-u}{2}$ and $\tilde{s} = \frac{z+u}{2}$ allows to formulate the functions I_1 and I_2 as

$$I_1(N_E, N_I) = \int_0^\infty \frac{e^{-\frac{s^2}{2}}}{s} (e^{s w_F} - e^{s w_R}) ds, \tag{3.5}$$

$$I_2(N_E, N_I) = \int_0^\infty \frac{e^{-\frac{s^2}{2}}}{s} (e^{s\tilde{w}_F} - e^{s\tilde{w}_R}) \, ds. \tag{3.6}$$

If $b_I^E = b_E^I = 0$ the equations are uncoupled, we are then reduced to the case of article [10]. The following theorem analyses the coupled case.

Theorem 3.1. *Assume that $b_I^E > 0, b_E^I > 0, \tau_E > 0, \tau_I > 0, a_\alpha(N_E, N_I) = a_\alpha$ constant, and $h^\alpha(v, N_E, N_I) = V_0^\alpha(N_E, N_I) - v$ with $V_0^\alpha(N_E, N_I) = b_E^\alpha N_E - b_I^\alpha N_I + (b_E^\alpha - b_E^E)v_{E,\text{ext}}$ for $\alpha = E, I$. Then there is always an odd number of steady states for (2.6) for both possible choices of $M_\alpha(t)$: $M_\alpha(t) = N_\alpha(t - \tau_\alpha)$ and $M_\alpha(t) = \frac{R_\alpha(t)}{\tau_\alpha}$.*

Moreover, if b_E^E is small enough or τ_E is large enough (in comparison with the rest of parameters), then there is a unique steady state for (2.6) for both choices of $M_\alpha(t)$.

Proof. The proof is based on determining the number of solutions of the system

$$1 = N_E (\tau_E + I_1(N_E, N_I)), \quad 0 < N_E < \frac{1}{\tau_E}, \tag{3.7}$$

$$1 = N_I (\tau_I + I_2(N_E, N_I)), \quad 0 < N_I < \frac{1}{\tau_I}. \tag{3.8}$$

With this aim, we adapt some ideas of [10, 11] to the system (3.7)–(3.8). Let us remember some of the most relevant properties of the functions I_1 and I_2 (see (3.5) and (3.6)), which were proved in [11]. I_1 satisfies:

1. $I_1(N_E, N_I)$ is C^∞ in both variables.
2. For every $N_E \in [0, \infty)$ fixed, $I_1(N_E, N_I)$ is an increasing strictly convex function on N_I , since for all integers $k \geq 1$

$$\frac{\partial^k I_1}{\partial N_I^k} = \left(\frac{b_E^I}{\sqrt{a_E}} \right)^k \int_0^\infty e^{-\frac{s^2}{2}} s^{k-1} (e^{s w_F} - e^{s w_R}) \, ds.$$

Thus, $\lim_{N_I \rightarrow \infty} I_1(N_E, N_I) = \infty$, for every $N_E \in [0, \infty)$ fixed.

3. For every $N_I \in [0, \infty)$ fixed, $I_1(N_E, N_I)$ is a decreasing convex function on N_E , since for all integers $k \geq 1$

$$\frac{\partial^k I_1}{\partial N_E^k} = (-1)^k \left(\frac{b_E^E}{\sqrt{a_E}} \right)^k \int_0^\infty e^{-\frac{s^2}{2}} s^{k-1} (e^{s w_F} - e^{s w_R}) \, ds.$$

Thus, $\lim_{N_E \rightarrow \infty} I_1(N_E, N_I) = 0$, for every $N_I \in [0, \infty)$ fixed.

And I_2 verifies:

1. $I_2(N_E, N_I)$ is C^∞ on both variables.
2. For every N_E fixed, $I_2(N_E, N_I)$ is an increasing strictly convex function on N_I , since for all integers $k \geq 1$

$$\frac{\partial^k I_2}{\partial N_I^k} = \left(\frac{b_I^I}{\sqrt{a_I}} \right)^k \int_0^\infty e^{-\frac{s^2}{2}} s^{k-1} (e^{s\tilde{w}_F} - e^{s\tilde{w}_R}) \, ds. \tag{3.9}$$

Thus, $\lim_{N_I \rightarrow \infty} I_2(N_E, N_I) = \infty$ for every N_E fixed.

3. If we consider $N_I \in [0, \infty)$, $I_2(N_E, N_I)$ is a decreasing convex function on N_E , since for all integers $k \geq 1$

$$\frac{\partial^k I_2}{\partial N_E^k} = (-1)^k \left(\frac{b_E^I}{\sqrt{a_I}} \right)^k \int_0^\infty e^{-\frac{s^2}{2}} s^{k-1} (e^{s\tilde{w}_F} - e^{s\tilde{w}_R}) \, ds. \quad (3.10)$$

Thus, $\lim_{N_E \rightarrow \infty} I_2(N_E, N_I) = 0$, for every N_I fixed.

4. Using expression (3.3) for I_2 , for every N_E fixed, $I_2(N_E, 0) < \infty$, since

$$I_2(N_E, 0) = \int_{-\infty}^{\tilde{w}_F(0)} e^{-\frac{\tilde{z}^2}{2}} \int_{\max(\tilde{z}, \tilde{w}_R(0))}^{\tilde{w}_F(0)} e^{\frac{\tilde{u}^2}{2}} \, d\tilde{u} \, d\tilde{z} \leq \sqrt{2\pi} \left(\frac{V_F - V_R}{\sqrt{a_I}} \right) e^{\frac{m}{2a_I}},$$

where $m = \max\{(V_F - b_E^I N_E - (b_E^I - b_E^E)v_{E,\text{ext}})^2, (V_R - b_E^I N_E - (b_E^I - b_E^E)v_{E,\text{ext}})^2\}$.

Now we are ready to tackle the issue of the number of solutions to the system (3.7)–(3.8).

- **Step 1.** For every $N_E > 0$ fixed, there is a unique solution $N_I(N_E)$ that solves (3.8). This happens due to the fact that for $N_E > 0$ fixed, the function $f(N_I) = N_I(\tau_I + I_2(N_E, N_I))$ satisfies: $f(0) = 0$, $f(\frac{1}{\tau_I}) = 1 + \frac{I_2(N_E, \frac{1}{\tau_I})}{\tau_I} > 1$ and that it is increasing, since $I_2(N_E, N_I)$ is an increasing, strictly convex function on N_I (property 2).
- **Step 2.** There is always an odd number of steady states. This step is a consequence of the fact that the function $\mathcal{F}(N_E) := N_E[I_1(N_E, N_I(N_E)) + \tau_E]$ satisfies that $\mathcal{F}(0) = 0$ and that $\mathcal{F}(\frac{1}{\tau_E}) = 1 + \frac{I_1(\frac{1}{\tau_E}, N_I(\frac{1}{\tau_E}))}{\tau_E} > 1$.
- **Step 3.** Values of the parameters that provide sufficient conditions for the uniqueness of the steady state. We analyze the derivative of \mathcal{F} :

$$\mathcal{F}'(N_E) = I_1(N_E, N_I(N_E)) + \tau_E + N_E \left[-\frac{b_E^E}{\sqrt{a_E}} + \frac{b_E^I}{\sqrt{a_E}} N_I'(N_E) \right] \int_0^\infty e^{-\frac{s^2}{2}} (e^{s\tilde{w}_F} - e^{s\tilde{w}_R}) \, ds.$$

It is non-negative for $0 < N_E < \frac{1}{\tau_E}$, for certain parameter values, and therefore there is a unique steady state in these cases. For b_E^E small, $\mathcal{F}'(N_E)$ is positive since all the terms are positive, because $N_I'(N_E)$ is positive (see the proof of Thm. 4.1 in [11]). For τ_E large, the proof of the positivity of $\mathcal{F}'(N_E)$ is more complicated. It is necessary to use

$$N_I'(N_E) = \frac{b_E^I N_I^2(N_E) I(N_E)}{\sqrt{a_I} + b_E^I N_I^2(N_E) I(N_E)}, \quad (3.11)$$

where

$$I(N_E) = \int_0^\infty e^{-s^2/2} e^{\frac{-(b_E^I N_E - b_E^I N_I(N_E)) + (b_E^I - b_E^E)v_{E,\text{ext}}s}{\sqrt{a_I}}} \left(e^{sV_F/\sqrt{a_I}} - e^{sV_R/\sqrt{a_I}} \right) \, ds.$$

This expression for $N_I'(N_E)$ is obtained differentiating (3.8) respect to N_E . The function $N_I(N_E)$ is increasing and $I(N_E)$ is decreasing, since $0 < N_I'(N_E) < \frac{b_E^I}{b_E^I}$ (see the proof of Thm. 4.1 in [11]). Therefore, for $0 < N_E < \frac{1}{\tau_E}$,

$$A < -\frac{b_E^E}{\sqrt{a_E}} + \frac{b_E^I}{\sqrt{a_E}} N_I'(N_E) < B,$$

where $A := -\frac{b_E^E}{\sqrt{a_E}} + \frac{b_I^E}{\sqrt{a_E}} \frac{b_E^I N_I^2(0) I(\frac{1}{\tau_E})}{\sqrt{a_I + b_I^I N_I^2(\frac{1}{\tau_E})} I(0)}$ and $B := -\frac{b_E^E}{\sqrt{a_E}} + \frac{b_I^E}{\sqrt{a_E}} \frac{b_E^I N_I^2(\frac{1}{\tau_E}) I(0)}{\sqrt{a_I + b_I^I N_I^2(0) I(\frac{1}{\tau_E})}}$. Thus, if $0 \leq A$ it is obvious that $\mathcal{F}(N_E)$ is increasing. For the case $A < 0$, some additional computations are needed. First, we consider $I_m := \min_{0 \leq N_E \leq \frac{1}{\tau_E}} I_1(N_E, N_I(N_E))$. Next, since $A < 0$,

$$I_m + \tau_E + \frac{A}{\tau_E} \tilde{I}(\tau_E) \leq \mathcal{F}'(N_E),$$

where $\tilde{I}(\tau_E) := \int_0^\infty e^{-\frac{s^2}{2}} e^{\frac{sb_I^E N_I(\frac{1}{\tau_E})}{\sqrt{a_E}}} \left(e^{\frac{sV_F}{\sqrt{a_E}}} - e^{\frac{sV_R}{\sqrt{a_E}}} \right) ds$. Finally, if $0 < I_m + \tau_E + \frac{A}{\tau_E} \tilde{I}(\tau_E)$, or equivalently $-A\tilde{I}(\tau_E) < \tau_E(I_m + \tau_E)$, then $\mathcal{F}(N_E)$ is increasing. We observe that it happens for τ_E large enough. □

Remark 3.2. Analyzing in more detail the expression of A in the previous proof ($A = -\frac{b_E^E}{\sqrt{a_E}} + \frac{b_I^E}{\sqrt{a_E}} \frac{b_E^I N_I^2(0) I(\frac{1}{\tau_E})}{\sqrt{a_I + b_I^I N_I^2(\frac{1}{\tau_E})} I(0)}$), we observe that for $b_E^I b_I^E$ large or b_I^I small enough, in comparison with the rest of parameters, there is also a unique stationary solution, since $A > 0$.

In other words, what we obtain is the uniqueness of the steady state in terms of the size of the parameters. More precisely: If one of the two pure connectivity parameters, b_E^E or b_I^I , is small, or one of the two cross connectivity parameters, b_E^I or b_I^E , is large, or the excitatory refractory period, τ_E , is large, then there exists a unique steady state.

3.1. Long time behavior

As proved in [11, 20], where no refractory states were considered, the solutions converge exponentially fast to the unique steady state when the connectivity parameters are small enough. We extend these results to the case where refractory states, but no delays, are included. We prove the result for the case of only one population in the following theorem, and then show the general case of two populations.

Theorem 3.3. Consider system (2.13) and $M(t) = \frac{R(t)}{\tau}$. Assume that the connectivity parameter b is small enough, $|b| \ll 1$, the diffusion term is constant, $a(N) = a$ for some $a > 0$, there is no transmission delay, $D = 0$, and that the initial datum is close enough to the unique steady state $(\rho_\infty, R_\infty, N_\infty)$,

$$\int_{-\infty}^{V_F} \rho_\infty(v) \left(\frac{\rho^0(v) - \rho_\infty(v)}{\rho_\infty(v)} \right)^2 dv + R_\infty \left(\frac{R(0)}{R_\infty} - 1 \right)^2 \leq \frac{1}{2|b|}. \tag{3.12}$$

Then, for fast decaying solutions to (2.13) there is a constant $\mu > 0$ such that for all $t \geq 0$

$$\int_{-\infty}^{V_F} \rho_\infty(v) \left(\frac{\rho(v) - \rho_\infty(v)}{\rho_\infty(v)} \right)^2 dv + \frac{(R(t) - R_\infty)^2}{R_\infty} \leq e^{-\mu t} \left[\int_{-\infty}^{V_F} \rho_\infty(v) \left(\frac{\rho^0(v) - \rho_\infty(v)}{\rho_\infty(v)} \right)^2 dv + \frac{(R^0 - R_\infty)^2}{R_\infty} \right].$$

Proof. The proof combines a relative entropy argument with the Poincaré’s inequality that is presented in ([10], Prop. 5.3). Additionally, to deal with the nonlinearity (the connectivity parameter does not vanish) we follow some ideas of ([20], Thm. 2.1). Notice that along the proof we will use the simplified notation

$$p(v, t) = \frac{\rho(v, t)}{\rho_\infty(v)}, \quad r(t) = \frac{R(t)}{R_\infty}, \quad \eta(t) = \frac{N(t)}{N_\infty}.$$

First, for any smooth convex function $G : \mathbb{R}^+ \rightarrow \mathbb{R}$, we recall that a natural relative entropy for equation (2.13) is defined as

$$E(t) := \int_{-\infty}^{V_F} \rho_\infty G(p(v, t)) \, dv + R_\infty G(r(t)). \tag{3.13}$$

The time derivative of the relative entropy (3.13) can be written as

$$\begin{aligned} \frac{d}{dt} E(t) &= -a \int_{-\infty}^{V_F} \rho_\infty(v) G''(p(v, t)) \left[\frac{\partial p}{\partial v} \right]^2 (v, t) \, dv \\ &\quad - N_\infty [G(\eta(t)) - G(p(V_R, t)) - (r(t) - p(V_R, t)) G'(p(V_R, t)) - (\eta(t) - r(t)) G'(r(t))] \\ &\quad + b(N(t) - N_\infty) \int_{-\infty}^{V_F} \frac{\partial \rho_\infty}{\partial v}(v) [G(p(v, t)) - p(v, t) G'(p(v, t))] \, dv. \end{aligned} \tag{3.14}$$

Expression (3.14) is achieved after some simple computations, taking into account that (ρ, R, N) is a solution of equation (2.13) and that $(\rho_\infty, R_\infty, N_\infty)$ is the unique steady state of the same equation, thus given by

$$\begin{cases} \frac{\partial}{\partial v} [h(v, N_\infty) \rho_\infty(v)] - a \frac{\partial^2 \rho_\infty}{\partial v^2}(v) = \frac{R_\infty}{\tau} \delta(v - V_R), \\ R_\infty = \tau N_\infty, \quad N_\infty = -a \frac{\partial \rho_\infty}{\partial v}(V_F) \geq 0, \\ \rho_\infty(-\infty) = 0, \quad \rho_\infty(V_F) = 0. \end{cases}$$

Specifically, we can obtain successively the following relations:

$$\frac{\partial p}{\partial t} - \left(v - bN + \frac{2a}{\rho_\infty} \frac{\partial \rho_\infty}{\partial v} \right) \frac{\partial p}{\partial v} - a \frac{\partial^2 p}{\partial v^2} = \frac{R_\infty}{\tau \rho_\infty} \delta(v - V_R) (r - p) - \frac{p}{\rho_\infty} b(N - N_\infty) \frac{\partial \rho_\infty}{\partial v}, \tag{3.15}$$

$$\begin{aligned} \frac{\partial G(p)}{\partial t} - \left(v - bN + \frac{2a}{\rho_\infty} \frac{\partial \rho_\infty}{\partial v} \right) \frac{\partial G(p)}{\partial v} - a \frac{\partial^2 G(p)}{\partial v^2} &= -G'(p) \frac{p}{\rho_\infty} b(N - N_\infty) \frac{\partial \rho_\infty}{\partial v} \\ &\quad - aG''(p) \left(\frac{\partial p}{\partial v} \right)^2 + G'(p) \frac{R_\infty}{\tau \rho_\infty} \delta(v - V_R) (r - p), \end{aligned} \tag{3.16}$$

and

$$\begin{aligned} \frac{\partial}{\partial t} \rho_\infty G(p) - \frac{\partial}{\partial v} [(v - bN) \rho_\infty G(p)] - a \frac{\partial^2}{\partial v^2} [\rho_\infty G(p)] &= b(N - N_\infty) \frac{\partial \rho_\infty}{\partial v} [G(p) - pG'(p)] - a \rho_\infty G''(p) \left(\frac{\partial p}{\partial v} \right)^2 \\ &\quad + \frac{R_\infty}{\tau} \delta(v - V_R) [(r - p) G'(p) + G(p)]. \end{aligned} \tag{3.17}$$

Finally, (3.14) is obtained after integrating (3.17) with respect to v , between $-\infty$ and V_F , taking into account that

$$a \frac{\partial}{\partial v} [\rho_\infty G(p)]_{v=V_F} = -N_\infty G(\eta),$$

due to the boundary condition at V_F and the l'Hopital rule, and adding

$$\frac{d}{dt}R_\infty G(r) = \frac{R_\infty}{\tau}R_\infty G'(r)(\eta - r). \tag{3.18}$$

To obtain the exponential rate of convergence stated in the theorem, we consider $G(x) = (x - 1)^2$ in (3.14). Its first term is negative and will provide the strongest control when combined with the Poincaré’s inequality. After some algebraical computations, the second term can be written as

$$\begin{aligned} & -N_\infty[G(\eta(t)) - G(p(V_R, t)) - (r(t) - p(V_R, t))G'(p(V_R, t)) - (\eta(t) - r(t))G'(r(t))] \\ & = -N_\infty[(r(t) - \eta(t))^2 + (r(t) - p(V_R, t))^2]. \end{aligned}$$

Applying the inequality $(a + b)^2 \geq \epsilon(a^2 - 2b^2)$, for $a, b \in \mathbb{R}$ and $0 < \epsilon < \frac{1}{2}$, we obtain

$$-N_\infty(r(t) - \eta(t))^2 \leq -\epsilon N_\infty(\eta(t) - 1)^2 + 2\epsilon N_\infty(r(t) - 1)^2. \tag{3.19}$$

Recalling the Poincaré’s inequality of ([10], Prop. 5.3), and in a similar way as in [20], for small connectivity parameters, there exists $\gamma > 0$ such that:

$$\int_{-\infty}^{V_F} \frac{(\rho - \rho_\infty)^2}{\rho_\infty} dv + \frac{(R - R_\infty)^2}{R_\infty} \leq \frac{1}{\gamma} \left[\int_{-\infty}^{V_F} \rho_\infty(v) \left[\frac{\partial p}{\partial v} \right]^2 (v, t) dv + N_\infty(r(t) - p(V_R, t))^2 \right], \tag{3.20}$$

thus

$$(r(t) - 1)^2 \leq \frac{1}{\gamma R_\infty} \int_{-\infty}^{V_F} \rho_\infty(v) \left[\frac{\partial p}{\partial v} \right]^2 (v, t) dv + \frac{N_\infty}{\gamma R_\infty} (r(t) - p(V_R, t))^2, \tag{3.21}$$

and therefore

$$2\epsilon N_\infty(r(t) - 1)^2 \leq \frac{2\epsilon N_\infty}{\gamma R_\infty} \int_{-\infty}^{V_F} \rho_\infty(v) \left[\frac{\partial p}{\partial v} \right]^2 (v, t) dv + \frac{2\epsilon N_\infty}{\gamma R_\infty} N_\infty(r(t) - p(V_R, t))^2. \tag{3.22}$$

Joining now estimates (3.19) and (3.22), choosing $0 < \epsilon < \frac{1}{2}$ such that $\frac{2\epsilon N_\infty}{\gamma R_\infty} < \min(\frac{a}{2}, \frac{1}{2})$ and denoting $C_0 := \epsilon N_\infty$ yields

$$\begin{aligned} & -N_\infty[G(\eta(t)) - G(p(V_R, t)) - (r(t) - p(V_R, t))G'(p(V_R, t)) - (\eta(t) - r(t))G'(r(t))] \\ & \leq -C_0 G(\eta(t)) + \frac{a}{2} \int_{-\infty}^{V_F} \rho_\infty(v) \left[\frac{\partial p}{\partial v} \right]^2 (v, t) dv - \frac{1}{2} N_\infty(r(t) - p(V_R, t))^2. \end{aligned} \tag{3.23}$$

The third term can be bounded in the same way as in [20]. Thus, for some $C > 0$ we have

$$\begin{aligned} & b(N(t) - N_\infty) \int_{-\infty}^{V_F} \frac{\partial \rho_\infty}{\partial v}(v) [G(p(v, t)) - p(v, t)G'(p(v, t))] dv \\ & \leq C(2b^2 + |b|)(\eta(t) - 1)^2 + a \int_{-\infty}^{V_F} \rho_\infty \left[\frac{\partial p}{\partial v} \right]^2 (v, t) dv \left(\frac{1}{2} + |b| \int_{-\infty}^{V_F} \rho_\infty(v) (p(v, t) - 1)^2 dv \right). \end{aligned} \tag{3.24}$$

Combining estimates (3.23) and (3.24) gives the bound

$$\begin{aligned} \frac{d}{dt} E(t) &\leq -C_0(\eta(t) - 1)^2 + C(2b^2 + |b|)(\eta(t) - 1)^2 - \frac{1}{2}N_\infty(r(t) - p(V_R, t))^2 \\ &\quad - a \int_{-\infty}^{V_F} \rho_\infty(v) \left[\frac{\partial p}{\partial v} \right]^2 (v, t) \, dv \left(1 - |b| \int_{-\infty}^{V_F} \rho_\infty(v)(p(v, t) - 1)^2 \, dv \right). \end{aligned} \tag{3.25}$$

Taking now b small enough such that $C(2b^2 + |b|) \leq C_0$ we obtain

$$\begin{aligned} \frac{d}{dt} E(t) &\leq -\tilde{C} \left[\int_{-\infty}^{V_F} \rho_\infty(v) \left[\frac{\partial p}{\partial v} \right]^2 (v, t) \, dv + N_\infty(r(t) - p(V_R, t))^2 \right] \\ &\quad - \frac{a}{2} \int_{-\infty}^{V_F} \rho_\infty(v) \left[\frac{\partial p}{\partial v} \right]^2 (v, t) \, dv \left(1 - 2|b| \int_{-\infty}^{V_F} \rho_\infty(v)(p(v, t) - 1)^2 \, dv \right) \\ &\leq -\mu E(t) - \frac{a}{2} (1 - 2|b|E(t)) \int_{-\infty}^{V_F} \rho_\infty(v) \left[\frac{\partial p}{\partial v} \right]^2 (v, t) \, dv, \end{aligned}$$

where Poincaré’s inequality (3.20) was used, with $\tilde{C} = \min(\frac{a}{2}, \frac{1}{2})$, $\mu = \tilde{C}\gamma$. Finally, thanks to the choice of the initial datum (3.12) and Gronwall’s inequality, the relative entropy decreases for all times so that, $E(t) \leq \frac{1}{2|b|}$, $\forall t \geq 0$, and the result is proved:

$$E(t) \leq e^{-\mu t} E(0) \leq e^{-\mu t} \frac{1}{2|b|}.$$

□

For two populations with refractory states (as given in model [10]), this exponential rate of convergence to the unique steady can also be proved. The proof is achieved by considering the full entropy for both populations:

$$\begin{aligned} \mathcal{E}[t] &:= \int_{-\infty}^{V_F} \rho_E^\infty(v) \left(\frac{\rho_E(v) - \rho_E^\infty(v)}{\rho_E^\infty(v)} \right)^2 \, dv + \int_{-\infty}^{V_F} \rho_I^\infty(v) \left(\frac{\rho_I(v) - \rho_I^\infty(v)}{\rho_I^\infty(v)} \right)^2 \, dv \\ &\quad + \frac{(R_E(t) - R_E^\infty)^2}{R_E^\infty} + \frac{(R_I(t) - R_I^\infty)^2}{R_I^\infty}, \end{aligned}$$

and proceeding in the same way as in ([11], Thm. 4.2), taking into account that now there are some terms with refractory states which have to be handled, as in Theorem 3.3.

Theorem 3.4. *Consider system (2.6) for two populations, with $M_\alpha(t) = \frac{R_\alpha(t)}{\tau_\alpha}$, $\alpha = I, E$. Assume that the connectivity parameters b_i^α are small enough, the diffusion terms $a_\alpha > 0$ are constant, the transmission delays D_i^α vanish ($\alpha = I, E$, $i = I, E$), and that the initial data (ρ_E^0, ρ_I^0) are close enough to the unique steady state $(\rho_E^\infty, \rho_I^\infty)$:*

$$\mathcal{E}[0] < \frac{1}{2 \max(b_E^E + b_I^E, b_E^I + b_I^I)}.$$

Then, for fast decaying solutions to (2.6), there is a constant $\mu > 0$ such that for all $t \geq 0$

$$\mathcal{E}[t] \leq e^{-\mu t} \mathcal{E}[0].$$

Consequently, for $\alpha = E, I$

$$\int_{-\infty}^{V_F} \rho_\alpha^\infty(v) \left(\frac{\rho_\alpha(v) - \rho_\alpha^\infty(v)}{\rho_\alpha^\infty(v)} \right)^2 dv + \frac{(R_\alpha(t) - R_\alpha^\infty)^2}{R_\alpha^\infty} \leq e^{-\mu t} \mathcal{E}[0].$$

In the previous results the delays were assumed to vanish, however a similar strategy could be considered for the model with delays to prove the exponential convergence. The problem in this case is that the second term of the right hand side of inequality (3.25) is transformed into $C(2b^2 + |b|)(\eta(t - D) - 1)^2$, and therefore should be compared to $C_0(\eta(t) - 1)^2$. It seems that the solutions also converge exponentially fast to the steady state for small nonzero values of the delays, since in these cases both terms might be compared. However, for larger values of the delay(s), it does not seem easy to ensure the negativity of the sum of both terms (as done in the proof of Thm. 3.3).

To conclude the study about the long time behavior we have to remember that solutions to (2.6) may blow-up in finite time if there are no delays. Specifically, following similar steps as those developed in ([10], Thm. 3.1) and ([11], Thm. 3.1), we can prove an analogous result for the general system (2.6) without delay between excitatory neurons, this is $D_E^E = 0$:

Theorem 3.5. *Assume that*

$$h^E(v, N_E, N_I) + v \geq b_E^E N_E - b_I^E N_I, \tag{3.26}$$

$$a_E(N_E, N_I) \geq a_m > 0, \tag{3.27}$$

$\forall v \in (-\infty, V_F]$, and $\forall N_I, N_E \geq 0$. Assume also that $D_E^E = 0$ and that there exists some $C > 0$ such that

$$\int_0^t N_I(s - D_I^E) ds \leq C t, \quad \forall t \geq 0. \tag{3.28}$$

Then, a weak solution to the system (2.6), for both possible choices of $M_\alpha(t)$: $M_\alpha(t) = N_\alpha(t - \tau_\alpha)$ and $M_\alpha(t) = \frac{R_\alpha(t)}{\tau_\alpha}$, cannot be global in time because one of the following reasons:

- $b_E^E > 0$ is large enough, for ρ_E^0 fixed.
- ρ_E^0 is ‘concentrated enough’ around V_F :

$$\int_{-\infty}^{V_F} e^{\mu v} \rho_E^0(v) dv \geq \frac{e^{\mu V_F}}{b_E^E \mu}, \quad \text{for a certain } \mu > 0 \tag{3.29}$$

and for $b_E^E > 0$ fixed.

Therefore, thanks to Theorems 3.4 and 3.5, we may conclude that, even with a unique steady state, if system (2.6) has immediate spike transmissions between excitatory neurons, (that is $D_E^E = 0$) then solutions can blow-up, whether initially they are close enough to the threshold potential or whether the excitatory neurons are highly connected (that is b_E^E is large enough). In the following numerical experiments we will show that the transmission delay between excitatory neurons prevent the blow-up phenomenon, but the rest of the transmission delays cannot avoid it.

4. NUMERICAL SCHEME

In this section we describe the deterministic numerical scheme that has been used to complete the theoretical analysis with numerical results. For simplicity in the explanation, we will focus on the one-population case, and only show how to extend it for two populations in the most difficult parts. Moreover, we recommend [45] for a

great review of numerical methods for conservation laws and [4, 13, 50, 51, 58] for other deterministic methods developed for related neural PDE models.

Let us consider the simplest NNLF model (2.13) as an example to describe this numerical solver. We first rewrite the equation as

$$\frac{\partial \rho}{\partial t}(v, t) = -\frac{\partial}{\partial v}[h(v, N(t-D))\rho(v, t)] + a(N)\frac{\partial^2 \rho}{\partial v^2}(v, t) + M(t)\delta(v - V_R),$$

and consider a uniform space mesh for $v \in I := [-V_{left}, V_F]$ given by $v_i = v_0 + i \, dv \, \forall i = 1, \dots, n$ and where $-V_{left}$ is chosen such that $\rho(-V_{left}, t) \sim 0$, since $\rho(-\infty, t) = 0$. Then, we approximate the two derivatives, the refractory states function $M(t)$ and the Dirac delta of the right hand side (RHS). The first derivative is approximated by a fifth order flux-splitting WENO scheme, as described below. The second derivative is approximated by standard second order finite differences and the Dirac delta by a very concentrated Maxwellian function.

To approximate the function $M(t)$ we have to distinguish two cases: $M(t) = N(t - \tau)$, whose value is recovered in the same manner as the delayed N , and $M(t) = \frac{R(t)}{\tau}$, which is approximated using a finite difference approximation of its ODE.

Thus, we denote by L the sum of all the approximations of the RHS, and write the approximated system as:

$$\begin{cases} \frac{\partial \rho}{\partial t}(v, t) = L(t, \rho(v, t)), & \forall t \geq 0, \quad \forall v \in I, \\ \rho(v, 0) = \rho^0(v), & \forall v \in I. \end{cases} \quad (4.1)$$

Finally, the time evolution of ρ is approximated by a third order TVD Runge-Kutta method, as described later. The time step is adapted dynamically *via* a Courant-Friedrichs-Lewy (CFL) condition.

Due to the delay, during the time evolution of the solution we have to recover the value of N at time $t - D$, for every time t . To implement this, we fix a time step \overline{dt} and define an array of $P = \frac{D}{\overline{dt}}$ positions. Therefore, this array will save only P values of $N(t)$ for a time interval $[kD, (k+1)D)$, $k = 0, 1, 2, \dots$. In the time interval $[(k+1)D, (k+2)D)$ these values of the array will be used to obtain the delayed values $N(t - D)$ by linear interpolation between the corresponding positions of the array. We assume that $N(t) = 0, \forall t < 0$, so initially all the values of the array are zero, and the recovered values for the first time interval ($k = 0$) are all zero. Notice that we use linear interpolation since the time step dt for the time evolution is taken according to the CFL condition.

The numerical approximation of the solution for the two-populations model was implemented using the same numerical scheme as that described above for one population. The main difference here is that the code runs over two cores using parallel computational techniques, following the ideas in [11]. Each core handles the equations of one of the populations. At the end of every time step the cores communicate *via* message passing interface (MPI) to exchange the values of the firing rates. Also, the transmission delays were handled as for one population, taking into account that now each processor has to save two arrays of firing rates, one for each population, since there are four different delays.

4.1. WENO scheme

Here, we summarize the WENO scheme [42, 67] for model (2.13). For the complete model (2.6), it runs the same way after taking into account that now there are two different fluxes: $h^\alpha(v, N_E(t - D_E^\alpha), N_I(t - D_I^\alpha))\rho_\alpha(v, t)$ for $\alpha = E, I$. These finite difference methods are suitable to approximate singular regions, as for instance, in semiconductor theory [16–18].

We consider the middle node mesh $v_{i+\frac{1}{2}} = v_0 + (i + \frac{1}{2}) \, dv$, and denote by $f(\rho(v, t)) = h(v, N(t - D))\rho(v, t)$. Thus, the first derivative of the advection term is approximated by centered finite differences using the middle nodes:

$$\frac{\partial}{\partial v}f(\rho(v, t)) \approx \frac{f(\rho(v_{i+\frac{1}{2}}, t)) - f(\rho(v_{i-\frac{1}{2}}, t))}{dv}, \quad \forall i = 1, \dots, n. \quad (4.2)$$

The WENO reconstruction permits to approximate the flux f on the middle nodes

$$\hat{f}_{i+\frac{1}{2}} \approx f(\rho(v_{i+\frac{1}{2}}, t)), \tag{4.3}$$

$$\hat{f}_{i-\frac{1}{2}} \approx f(\rho(v_{i-\frac{1}{2}}, t)), \tag{4.4}$$

by means of the v_i nodes: $\bar{f}_i = f(\rho(v_i, t))$, as we show below.

Moreover, depending on the direction of the “wind” or *Roe speed*: $\bar{a}_{i+\frac{1}{2}} \equiv \frac{\bar{f}_{i+1} - \bar{f}_i}{\rho_{i+1} - \rho_i}$, (4.3) is computed using the approximation on the right or the left of the flux on the middle node $v_{i+\frac{1}{2}}$. Specifically:

- If $\bar{a}_{i+\frac{1}{2}} \geq 0$ then the wind blows from the left to the right, and thus the approximation on the left is used: $\hat{f}_{i+\frac{1}{2}} = f_{i+\frac{1}{2}}^-$.
- If $\bar{a}_{i+\frac{1}{2}} < 0$ then the wind blows from the right to the left, and thus the approximation on the right is used: $\hat{f}_{i+\frac{1}{2}} = f_{i+\frac{1}{2}}^+$.

Finally, let us remember the concrete formulation of the fifth order WENO method [67]. The approximation on the left is

$$\hat{f}_{i+\frac{1}{2}}^- = \omega_0 f_{i+\frac{1}{2}}^{(0)} + \omega_1 f_{i+\frac{1}{2}}^{(1)} + \omega_2 f_{i+\frac{1}{2}}^{(2)}, \tag{4.5}$$

where the nonlinear weights ω_r are $\omega_r = \frac{\alpha_r}{\sum_{s=0}^2 \alpha_s}$, for $r = 0, 1, 2$, and the linear weights α_s are given by

$$\alpha_s = \frac{d_s}{(\epsilon + \beta_s)^2} \quad s = 0, 1, 2, \quad \epsilon = 10^{-6}, \quad d_0 = \frac{3}{10}, \quad d_1 = \frac{3}{5}, \quad d_2 = \frac{1}{10},$$

with the smoothness indicators β_s

$$\begin{aligned} \beta_0 &= \frac{13}{12}(\bar{f}_i - 2\bar{f}_{i+1} + \bar{f}_{i+2})^2 + \frac{1}{4}(3\bar{f}_i - 4\bar{f}_{i+1} + \bar{f}_{i+2})^2, \\ \beta_1 &= \frac{13}{12}(\bar{f}_{i-1} - 2\bar{f}_i + \bar{f}_{i+1})^2 + \frac{1}{4}(\bar{f}_{i-1} - \bar{f}_{i+1})^2, \\ \beta_2 &= \frac{13}{12}(\bar{f}_{i-2} - 2\bar{f}_{i-1} + \bar{f}_i)^2 + \frac{1}{4}(\bar{f}_{i-2} - 4\bar{f}_{i-1} + 3\bar{f}_i)^2. \end{aligned} \tag{4.6}$$

Finally, the third order fluxes are given by

$$\begin{aligned} f_{i+\frac{1}{2}}^{(0)} &= \frac{1}{3}\bar{f}_i + \frac{5}{6}\bar{f}_{i+1} - \frac{1}{6}\bar{f}_{i+2}, \\ f_{i+\frac{1}{2}}^{(1)} &= -\frac{1}{6}\bar{f}_{i-1} + \frac{5}{6}\bar{f}_i + \frac{1}{3}\bar{f}_{i+1}, \\ f_{i+\frac{1}{2}}^{(2)} &= \frac{1}{3}\bar{f}_{i-2} - \frac{7}{6}\bar{f}_{i-1} + \frac{11}{6}\bar{f}_i. \end{aligned}$$

In a similar way, the approximation on the right reads

$$\hat{f}_{i+\frac{1}{2}}^+ = \bar{\omega}_0 \bar{f}_{i+\frac{1}{2}}^{(0)} + \bar{\omega}_1 \bar{f}_{i+\frac{1}{2}}^{(1)} + \bar{\omega}_2 \bar{f}_{i+\frac{1}{2}}^{(2)}, \tag{4.7}$$

where the nonlinear weights $\bar{\omega}_r$ and the linear weights $\bar{\alpha}_s$ are given by

$$\bar{\omega}_r = \frac{\bar{\alpha}_r}{\sum_{s=0}^2 \bar{\alpha}_s} \quad r = 0, 1, 2, \quad \bar{\alpha}_s = \frac{\bar{d}_s}{(\epsilon + \beta_s)^2} \quad s = 0, 1, 2, \quad \epsilon = 10^{-6} \quad \bar{d}_0 = \frac{1}{10}, \quad \bar{d}_1 = \frac{3}{5}, \quad \bar{d}_2 = \frac{3}{10},$$

where the smoothness indicators β_s are defined by (4.6) and the third order fluxes are given by

$$\begin{aligned} \bar{f}_{i+\frac{1}{2}}^{(0)} &= \frac{11}{6} \bar{f}_{i+1} - \frac{7}{6} \bar{f}_{i+2} + \frac{1}{3} \bar{f}_{i+3}, \\ \bar{f}_{i+\frac{1}{2}}^{(1)} &= \frac{1}{3} \bar{f}_i + \frac{5}{6} \bar{f}_{i+1} - \frac{1}{6} \bar{f}_{i+2}, \\ \bar{f}_{i+\frac{1}{2}}^{(2)} &= -\frac{1}{6} \bar{f}_{i-1} + \frac{5}{6} \bar{f}_i + \frac{1}{3} \bar{f}_{i+1}. \end{aligned}$$

4.2. Flux-splitting WENO scheme

Among others an inconvenient of the WENO-Roe approximation is, that sometimes it leads to solutions that violate the entropy, as explained in [67]. This can be avoided, using a global *flux-splitting*. For that purpose, the flux is split using a suitable flux-splitting $f(\rho(v, t)) = f_{pos}(\rho(v, t)) + f_{neg}(\rho(v, t))$, which has to satisfy

$$\frac{d}{d\rho} f_{pos}(\rho(v, t)) \geq 0, \quad \frac{d}{d\rho} f_{neg}(\rho(v, t)) \leq 0.$$

The flux-splitting considered in this paper is the Lax-Friedrich splitting [67]

$$f_{pos}(\rho) = \frac{1}{2}(f(\rho) + \alpha\rho), \quad f_{neg}(\rho) = \frac{1}{2}(f(\rho) - \alpha\rho), \quad \text{where } \alpha = \max_{\rho} |f'(\rho)|.$$

In our case $f(\rho) = h(v, N)\rho$, and thus $\alpha = \max_{v \in (-\infty, V_F)} |h(v, N)|$.

Then the first derivative of the flux is calculated without using the Roe speed as

$$\frac{\partial f}{\partial v}(\rho(v_i, t)) \approx \frac{\hat{f}_{i+\frac{1}{2}} - \hat{f}_{i-\frac{1}{2}}}{dv}, \quad \forall i = 1, \dots, n, \tag{4.8}$$

where $\hat{f}_{i+\frac{1}{2}} = \hat{f}_{pos, i+\frac{1}{2}}^- + \hat{f}_{neg, i+\frac{1}{2}}^+$. Notice that $\hat{f}_{pos, i+\frac{1}{2}}^-$ is obtained applying (4.5) to the splitted flux f_{pos} and $\hat{f}_{neg, i+\frac{1}{2}}^+$ is calculated as (4.7) using f_{neg} as flux.

4.3. TVD third order Runge-Kutta method

The evolution in time of the solution of (4.1) is approximate by a third order TVD Runge-Kutta method as in [13, 68]:

$$\begin{aligned} \rho^{(1)} &= \rho^n + dtL(t_n, \rho^n), \\ \rho^{(2)} &= \frac{3}{4}\rho^n + \frac{1}{4}\rho^{(1)} + \frac{1}{4}dtL(t_n + dt, \rho^{(1)}), \\ \rho^{n+1} &= \frac{1}{3}\rho^n + \frac{2}{3}\rho^{(2)} + \frac{2}{3}dtL(t_n + 1/2dt, \rho^{(2)}), \end{aligned}$$

where dt denotes the time step, $\rho^n \equiv \rho(v, t_n)$ for $n = 0, 1, 2, \dots$ and $t_n = ndt$. Thus, for (flux-splitting) WENO it reads for $i = 1, \dots, n$

$$L(t, \rho(v_i, t)) \approx a \frac{\rho(v_{i+1}, t) - 2\rho(v_i, t) + \rho(v_{i-1}, t)}{dv^2} - \frac{\hat{f}_{i+\frac{1}{2}}(t) - \hat{f}_{i-\frac{1}{2}}(t)}{dv} + N(t)\delta(v_i - V_R),$$

where the Dirac delta is approximated by a Maxwellian function that is very concentrated on V_R .

In all the simulations done in this work the time step has been adapted dynamically by the CFL condition, thus for one population models, for every time the next time step is given by

$$dt \leq \min \left\{ \frac{adv^2}{2}, \frac{CFL dv}{\max_i \{|h(v_i, N(t - D))\}} \right\},$$

and for two population models by

$$dt \leq \min \left\{ \frac{a_E dv^2}{2}, \frac{a_I dv^2}{2}, \frac{CFL dv}{\max_i \{|h^E(v_i, N_E(t - D_E^\alpha), N_I(t - D_I^\alpha))\}}, \frac{CFL dv}{\max_i \{|h^I(v_i, N_E(t - D_E^\alpha), N_I(t - D_I^\alpha))\}} \right\}.$$

5. NUMERICAL RESULTS

In this section we present the numerical experiments that we have performed using the solver described in the previous section. These experiments, on the one hand, illustrate the analytical results, and on the other hand, they help to better understand some theoretical aspects that have not been solved until now. Among these problems, we highlight the stability of the steady states, the analysis of the behavior of the solutions when there is a nonzero delay in the excitatory-to-excitatory synapses, and the appearance of periodic solutions.

Thus, unless otherwise specified, for the showed simulations we will consider $V_F = 2$, $V_R = 1$, $\nu_{E,ext} = 0$, $a_\alpha(N_E, N_I) = 1$ and two different types of initial condition:

$$\rho_\alpha^0(v) = \frac{k}{\sqrt{2\pi}} e^{-\frac{(v-v_0^\alpha)^2}{2\sigma_0^{\alpha 2}}}, \tag{5.1}$$

where k is a constant such that $\int_{-V_{Ieft}}^{V_F} \rho_\alpha^0(v) dv \approx 1$ numerically, and

$$\rho_\alpha^0(v) = \frac{N_\alpha}{a_\alpha(N_E, N_I)} e^{-\frac{(v-V_0^\alpha(N_E, N_I))^2}{2a_\alpha(N_E, N_I)}} \int_{\max(v, V_R)}^{V_F} e^{-\frac{(w-V_0^\alpha(N_E, N_I))^2}{2a_\alpha(N_E, N_I)}} dw, \quad \alpha = E, I, \tag{5.2}$$

with $V_0^\alpha(N_E, N_I) = b_E^\alpha N_E - b_I^\alpha N_I + (b_E^\alpha - b_E^E)\nu_{E,ext}$ and where N_α is an approximated value of the stationary firing rate. The second kind of initial data is an approximation of the steady states of the system and allows us to study their local stability. Notice that we will also refer to (5.1) as the initial condition for the one-population model by considering $\rho_\alpha = \rho$, $v_0^\alpha = v_0$ and $\sigma_0^{\alpha 2} = \sigma_0^2$.

5.1. Analysis of the number of steady states

As a first step in our numerical analysis we illustrate numerically some of the results of Theorem 3.1. Figure 1 shows the behaviour of $\mathcal{F}(N_E) := N_E[I_1(N_E, N_I(N_E) + \tau_E)]$ for different parameter values, which produces bifurcation diagrams. In the figure on the left we observe the influence of the excitatory refractory period τ_E , considering fixed the rest of parameters; a large τ_E gives rise to the uniqueness of the steady state. And on the

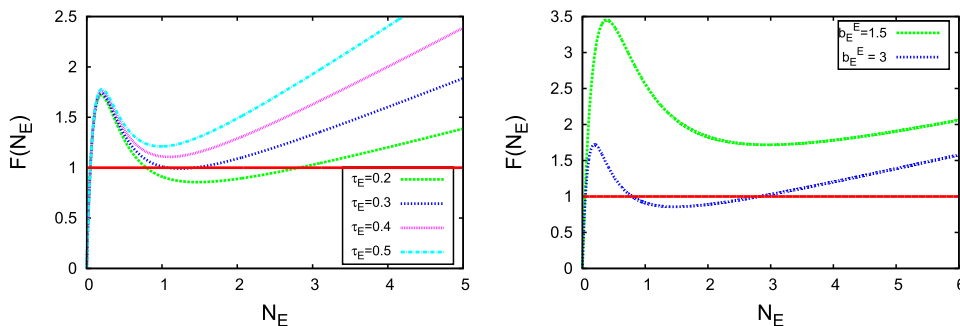


FIGURE 1. Number of steady states for system (2.6) described by Theorem 3.1. *Left:* For fixed $b_I^E = 7$, $b_I^I = 2$, $b_E^I = 0.01$, $b_E^E = 3$ and $\tau_I = 0.2$, we observe the influence of the excitatory refractory period τ_E . *Right:* For fixed $b_I^E = 7$, $b_I^I = 2$, $b_E^I = 0.01$ and $\tau_E = \tau_I = 0.2$, we observe the influence of the connectivity parameter b_E^E .

right, the impact of the connectivity parameter b_E^E is described. In this case, a small b_E^E guarantees a unique stationary solution. Moreover, as noted in Remark 3.2, we observe the uniqueness of the steady state if the system is highly connected between excitatory and inhibitory neurons, or if the excitatory neurons have a large enough refractory period.

As happens in the case of only one population [10], for two populations (excitatory and inhibitory), neurons in a refractory state guarantee the existence of stationary states. However, the refractory state itself does not prevent the blow-up phenomenon, as shown in Theorem 3.5 and Figures 4–6.

5.2. Blow-up

In [10], the blow-up phenomenon for one population of neurons with refractory states was shown. Theorem 3.5 extends this result to two populations of neurons, one excitatory and the other one inhibitory. The refractory period is not enough to avoid the blow-up of the network; if the membrane potentials of the excitatory population are close to the threshold potential, or if the connectivity parameter b_E^E is large enough, then the network blows-up in finite time. To achieve the global-in-time existence, it seems necessary some transmission delay between excitatory neurons, as we observe in our simulations and as it was proved at the microscopic level for one population [25].

We start the analysis of the blow-up phenomenon by considering only one average-excitatory population (we recall that there is global existence for one average-inhibitory population, see [19]). In [10, 12] it was proved that some solutions blow-up. In Figures 2 and 3, we show how the transmission delay of the spikes between neurons prevents the network from blowing-up in finite time, even in the case where the system has no steady states. Recall that the one population model without refractory states has no equilibria for large values of the connectivity parameter [12]. Initially, for this case, we expected a periodic behavior of the solutions after avoiding the blow-up, nevertheless, this does not happen, and the firing rate seems to increase, but not to blow-up in finite time (Fig. 2, *bottom*).

In [11], the excitatory-inhibitory system without refractory states was studied. In the current paper, we extend this analysis to the presence of refractory states. Figures 4 and 5 illustrate the results of Theorem 3.5; if there is no transmission delay between excitatory neurons, the solution blows-up because most of the excitatory neurons have a membrane potential close to the threshold potential, or because excitatory neurons are highly connected, that is, b_E^E is large enough. We observe in Figure 6 that the remaining delays do not avoid the blow-up phenomenon, since in this figure all the delays are 0.1, except $D_E^E = 0$. The importance of D_E^E is discerned in Figure 7. We show the evolution in time of the solution of (2.6), with the same initial data as considered in Figure 5 and with $D_E^E = 0.1$; in this case, the solution exists for every time, thus avoiding the blow-up.

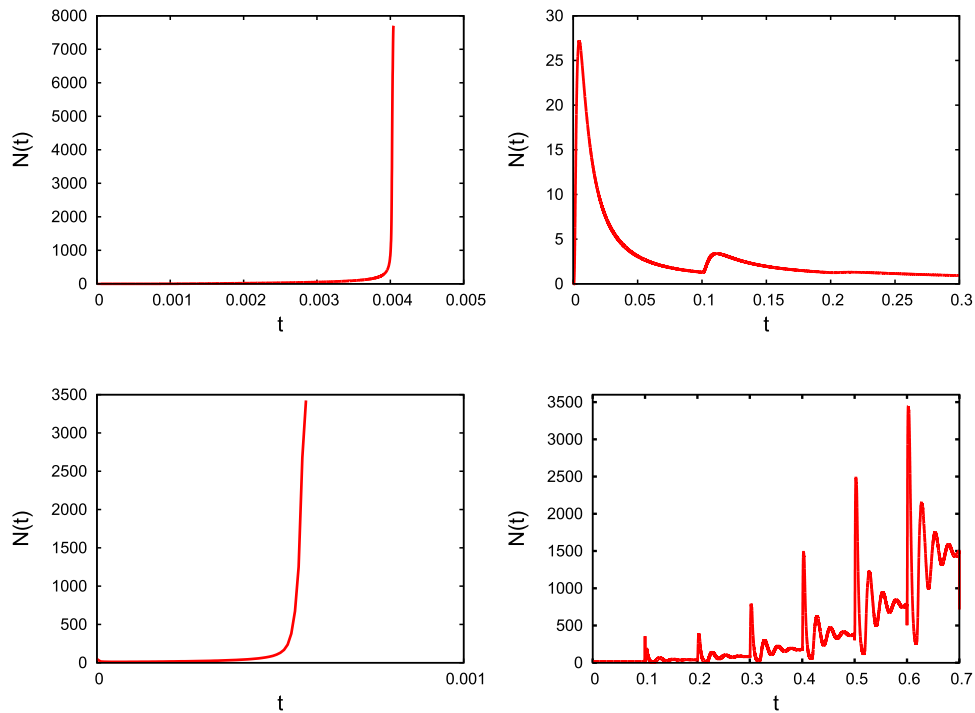


FIGURE 2. System (2.13) (only one population without refractory states) presents blow-up, if there is no transmission delay. We consider the initial data (5.1) with $v_0 = 1.83$. *Top:* $\sigma_0 = 0.0003$ and the connectivity parameter $b = 0.5$. *Left:* N blows-up in finite time, if there is no delay, $D = 0$. *Right:* N tends to a steady state, if there is delay, $D = 0.1$. *Bottom:* $\sigma_0 = 0.003$ and the connectivity parameter $b = 2.2$. *Left:* N blows-up in finite time, if there is no delay, $D = 0$. *Right:* N does not blow-up if there is delay, $D = 0.1$.

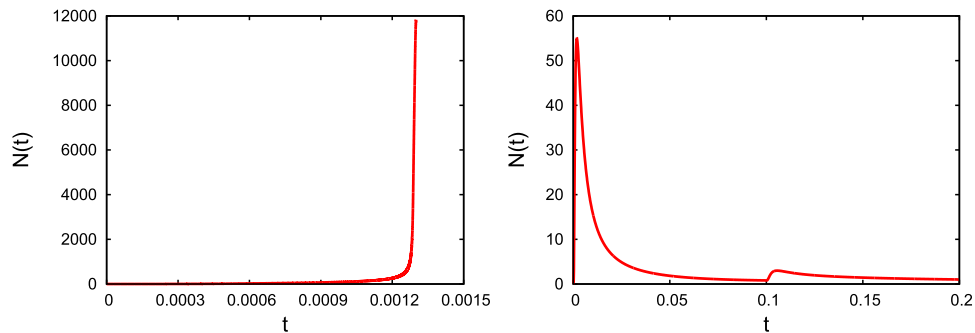


FIGURE 3. System (2.13) (only one population with refractory state: $M(t) = \frac{R(t)}{\tau}$) presents blow-up, if there is no transmission delay. We consider the initial data (5.1) with $v_0 = 1.83$, and $\sigma_0 = 0.0003$, and the connectivity parameter $b = 0.5$. *Left:* $R(0) = 0.2$, $\tau = 0.025$ and $D = 0$, since there is no transmission delay N blows-up in finite time. *Right:* $R(0) = 0.2$, $\tau = 0.025$ and $D = 0.07$, the solution tends to the steady state, due to the transmission delay.

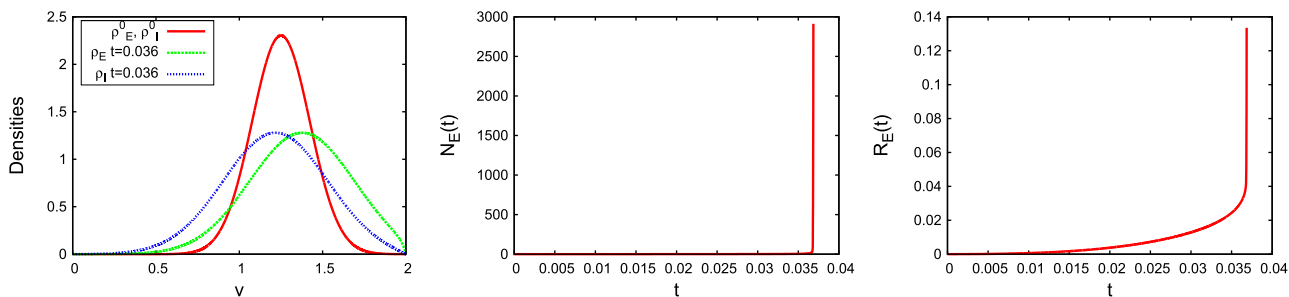


FIGURE 4. System (2.6) (two populations: excitatory and inhibitory) presents blow-up, if there are no transmission delays. We consider initial data (5.1) with $v_0^E = v_0^I = 1.25$ and $\sigma_0^E = \sigma_0^I = 0.0003$, the connectivity parameters $b_E^E = 6$, $b_I^E = 0.75$, $b_I^I = 0.25$, $b_E^I = 0.5$, and with refractory states ($M_\alpha(t) = N_\alpha(t - \tau_\alpha)$) where $\tau_\alpha = 0.025$. We observe that the initial data are not concentrated around the threshold potential but the solution blows-up because $b_E^E = 6$ is large enough and there are no transmission delays (see Thm. 3.5).

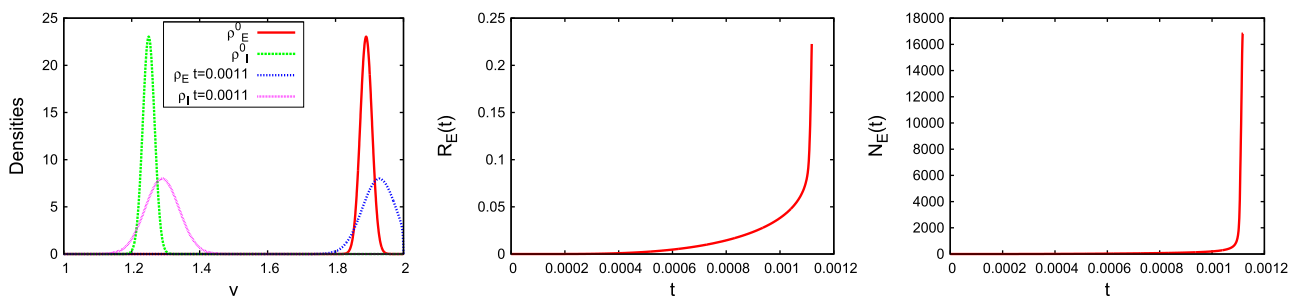


FIGURE 5. System (2.6) (two populations: excitatory and inhibitory) presents blow-up, if there are no transmission delays. We consider initial data (5.1) with $v_0^E = 1.89$, $v_0^I = 1.25$ and $\sigma_0^E = \sigma_0^I = 0.0003$, the connectivity parameters $b_E^E = 0.5$, $b_I^E = 0.75$, $b_I^I = 0.25$, $b_E^I = 0.5$, and with refractory states ($M_\alpha(t) = N_\alpha(t - \tau_\alpha)$) where $\tau = 0.025$. We observe that $b_E^E = 0.5$ is not large enough, but the solution blows-up because the initial condition for the excitatory population is concentrated around the threshold potential and there are no transmission delay (see Thm. 3.5).

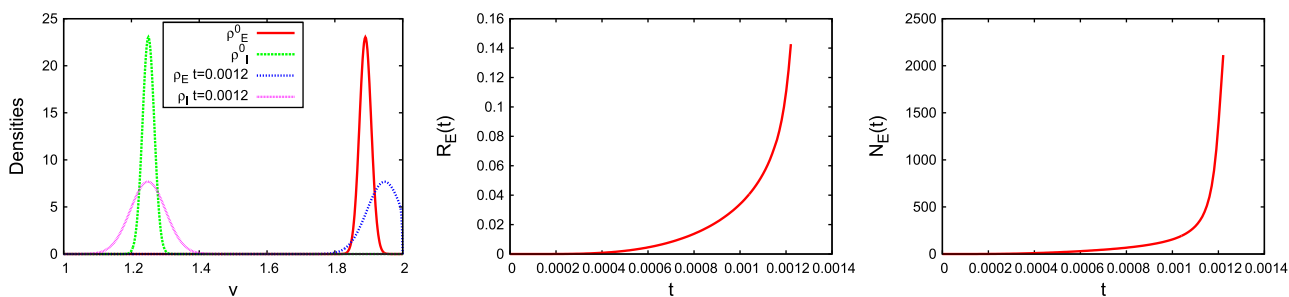


FIGURE 6. System (2.6) (two populations: excitatory and inhibitory) presents blow-up, if there is no excitatory transmission delay. We consider initial data (5.1) with $v_0^E = 1.89$, $v_0^I = 1.25$ and $\sigma_0^E = \sigma_0^I = 0.0003$, the connectivity parameters $b_E^E = 0.5$, $b_I^E = 0.75$, $b_I^I = 0.25$, $b_E^I = 0.5$, and with refractory states ($M_\alpha(t) = N_\alpha(t - \tau_\alpha)$) where $\tau_\alpha = 0.025$. All the delays are 0.1, except $D_E^E = 0$. We observe that the other delays do not avoid the blow-up due to a concentrated initial condition for the excitatory population.

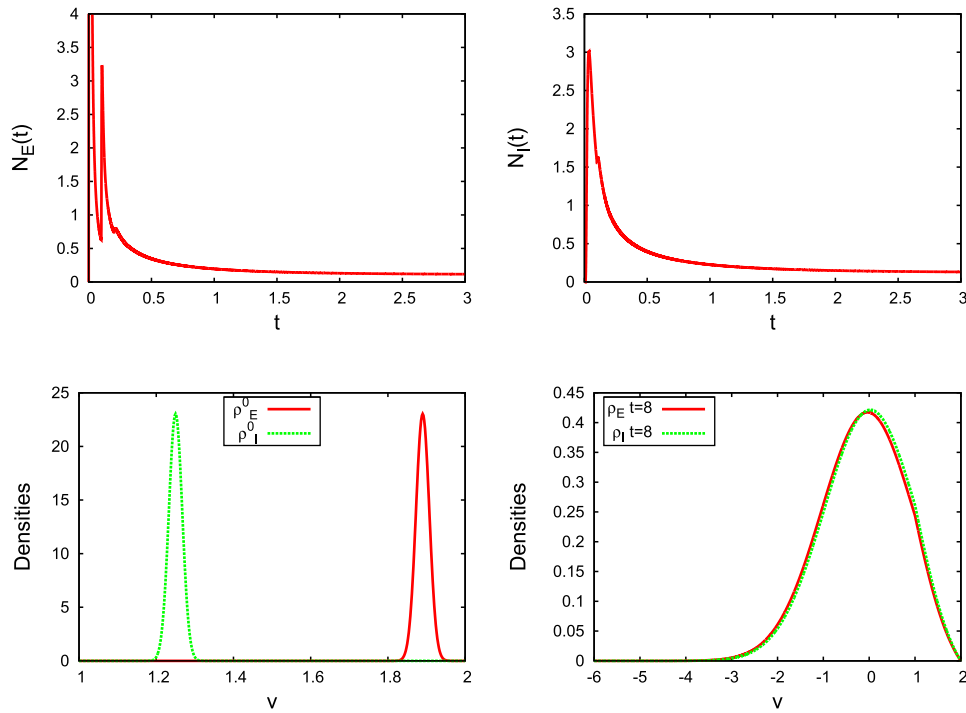


FIGURE 7. System (2.6) (two populations: excitatory and inhibitory) avoids blow-up, if there is a transmission delay between excitatory neurons. We consider initial data (5.1) with $v_0^E = 1.89$, $v_0^I = 1.25$ and $\sigma_0^E = \sigma_0^I = 0.0003$, the connectivity parameters $b_E^E = 0.5$, $b_I^E = 0.75$, $b_I^I = 0.25$, $b_E^I = 0.5$, $D_E^I = D_I^E = D_I^I = 0$, and with refractory states ($M_\alpha(t) = N_\alpha(t - \tau_\alpha)$) where $\tau = 0.025$. We observe that if there is a transmission delay between excitatory neurons $D_E^E = 0.1$, the blow-up phenomenon is avoided. *Top*: Firing rates. *Bottom*: Probability densities.

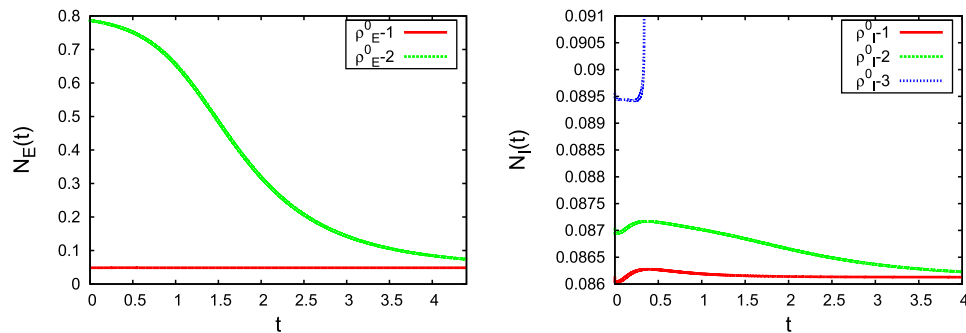


FIGURE 8. Numerical analysis of the stability in the case of three steady states for the system (2.6). If $b_I^E = 7$, $b_I^I = 2$, $b_E^I = 0.01$, $\tau_E = \tau_I = 0.2$ and $b_E^E = 3$, there are three steady states (see Fig. 1). The initial conditions for this simulations, $\rho_\alpha^0 - 1, 2, 3$, are given by the profile (5.2), where N_α are approximations of the stationary firing rates. We show the evolution of the excitatory and inhibitory firing rates and observe that the lowest steady state is stable and the other two are unstable.

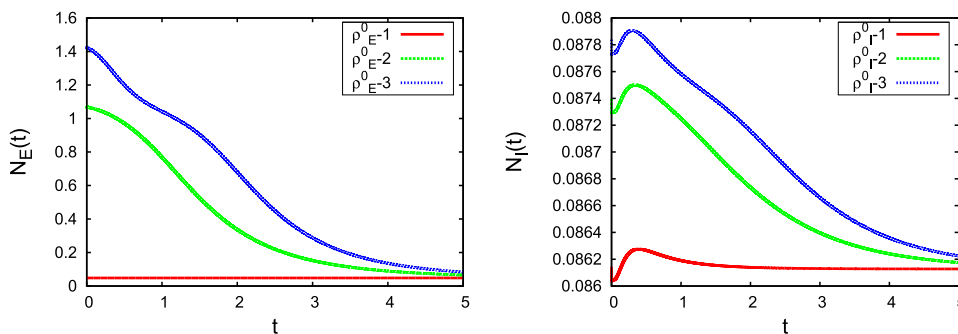


FIGURE 9. Numerical analysis of the stability in the case of three steady states for the system (2.6). If $b_I^E = 7$, $b_I^I = 2$, $b_E^I = 0.01$, $\tau_E = 0.3$, $\tau_I = 0.2$ and $b_E^E = 3$, there are three steady states (see Fig. 1). The initial conditions used for this simulations, $\rho_\alpha^0 - 1, 2, 3$, are given by the profile (5.2), where N_α are approximations of the stationary firing rates. We show the evolution of the excitatory and inhibitory firing rates and observe that the lowest steady state is stable and the other two are unstable.

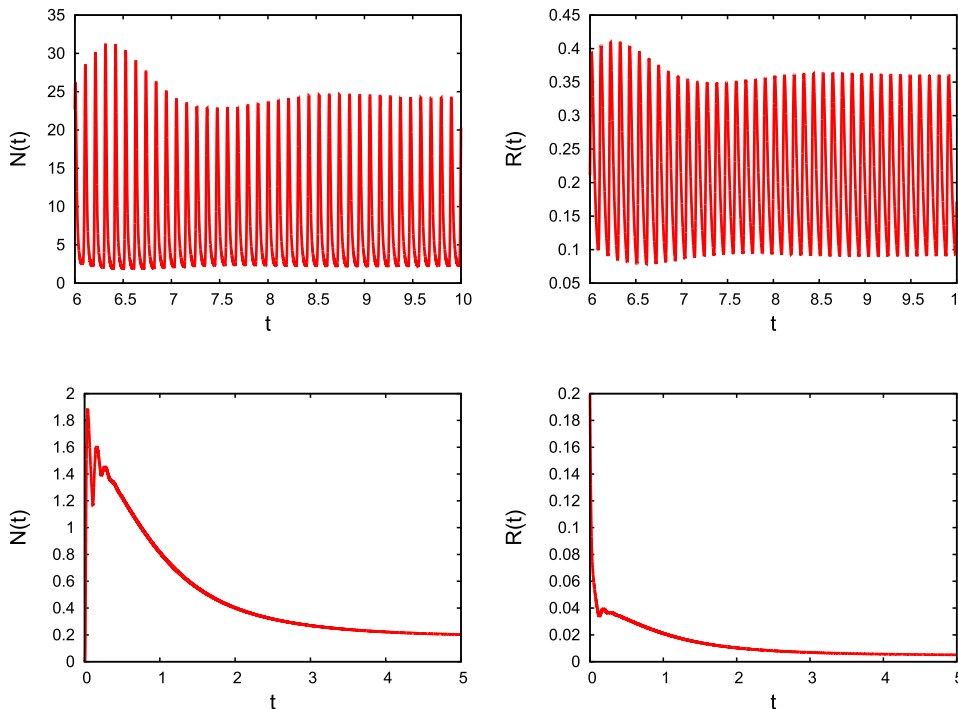


FIGURE 10. System (2.13) (only one average-excitatory population) presents periodic solutions, if there is a transmission delay. We consider initial data (5.1) with $\sigma_0 = 0.0003$, the connectivity parameter $b = 1.5$, the transmission delay $D = 0.1$, $v_{\text{ext}} = 0$ and with refractory states ($M(t) = \frac{R(t)}{\tau}$), where $\tau = 0.025$ and $R(0) = 0.2$. Periodic solutions appear if the initial condition is concentrated enough around the threshold potential *Top*: $v_0 = 1.83$. *Bottom*: $v_0 = 1.5$.

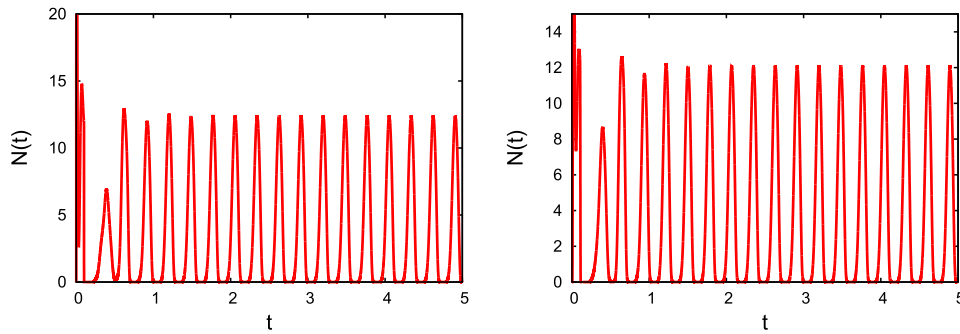


FIGURE 11. System (2.13) (only one average-inhibitory population) presents periodic solutions, if there is a transmission delay. We consider initial data (5.1) with $\sigma_0 = 0.0003$, the connectivity parameter $b = -4$, the transmission delay $D = 0.1$, and with refractory states ($M(t) = \frac{R(t)}{\tau}$), where $\tau = 0.025$ and $R(0) = 0.2$. Periodic solutions appear if the initial condition is concentrated enough around the threshold potential, but even if the initial datum is far from the threshold and the v_{ext} is large. *Left:* $v_0 = 1.83$, $v_{\text{ext}} = 20$. *Right:* $v_0 = 1.5$, $v_{\text{ext}} = 20$.

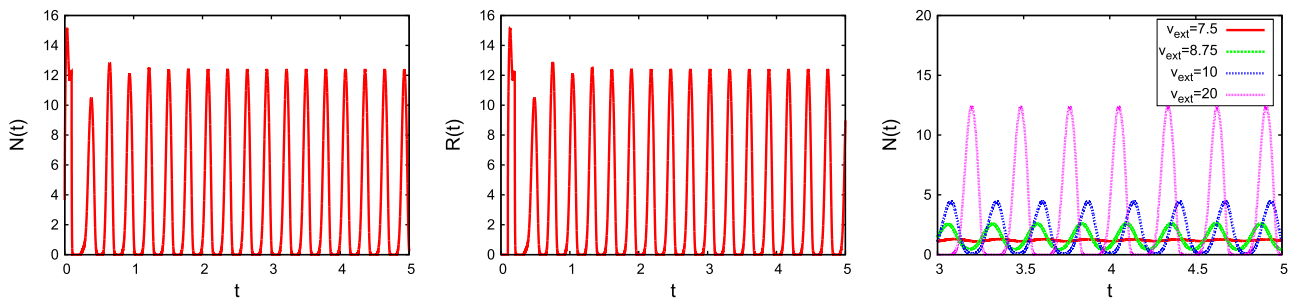


FIGURE 12. System (2.13) (only one average-inhibitory population) presents periodic solutions, if there is a transmission delay. We consider initial data (5.2) with $N = 3.669$, the connectivity parameter $b = -4$, the transmission delay $D = 0.1$, $v_{\text{ext}} = 20$ and with refractory states ($M(t) = \frac{R(t)}{\tau}$), where $\tau = 0.025$ and $R(0) = 0.091725$. Periodic solutions also appear if the initial condition is very close to the unique equilibrium when v_{ext} is large. Indeed, for this parameter space, solutions always converge to the same periodic solution. *Left* and *center*: Evolution of the firing rate and the refractory state for the solution with initial data given by (5.2) with firing rate $N = 3.669$. *Right*: Influence of v_{ext} in the behaviour of the system.

5.3. Steady states and periodic solutions

In Figure 1 we examined several choices of the model parameters, for which the system (2.6) presents three steady states. For one of these cases, the analysis of their stability is numerically investigated in Figure 8. For $\alpha = E, I$, the initial conditions $\rho_\alpha^0 - 1, 2, 3$ are given by the profiles (5.2), where N_α are approximations of the stationary firing rates. The evolution in time of the firing rates show that the lower steady state seems to be stable, while the two others are unstable. Moreover, considering as initial data (5.2) with N_α approximations of the higher stationary firing rates the solution blows-up in finite time, while with the intermediate firing rate the solution tends to the lower steady state. Figure 9 also describes the stability when there are three steady states. In this case the intermediate state is very close to the highest one. Here, the lower steady state also appears to be stable. The two others are unstable, but the higher one does not blow-up in finite time.

The transmission delay not only prevents the blow-up phenomenon, but also can produce periodic solutions. In Figure 10, we analyze the influence of the transmission delay for one average-excitatory population; if the

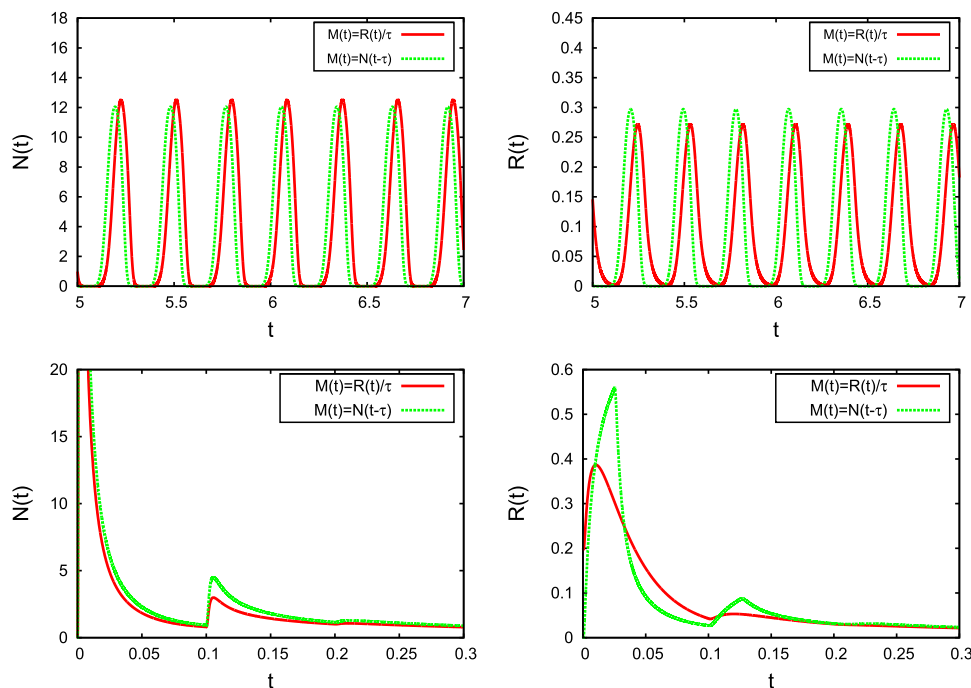


FIGURE 13. Comparison between $R(t)$ and $N(t)$ for $M(t) = \frac{R(t)}{\tau}$ and $M(t) = N(t - \tau)$. *Top*: Initial data (5.1) with $v_0 = 1.83$ and $\sigma_0 = 0.0003$, the connectivity parameter $b = -4$, the transmission delay $D = 0.1$, $\tau = 0.025$, $R(0) = 0.2$ and $v_{\text{ext}} = 20$. *Bottom*: Parameter space of Figure 3, bottom. The qualitative behavior is the same for both models, even the solutions seem to be hardly the same.

initial datum is concentrated around V_F , periodic solutions appear; on the contrary, if it is far from V_F , the solution reaches a steady state. In Figures 11 and 12, for one average-inhibitory population with transmission delay, we show that periodic solutions emerge if the initial condition is concentrated around the threshold potential, and even if the initial datum is far from the threshold and v_{ext} is large. A comparison between $R(t)$ and $N(t)$ for $M(t) = \frac{R(t)}{\tau}$ and $M(t) = N(t - \tau)$ is presented in Figure 13. In both cases the steady state is the same and the solutions tend to it. If the system tends to a synchronous state, these states are also almost the same for both possible choices of M .

Synchronous states appear also in the case of two populations (excitatory and inhibitory), as it is described in Figure 14. In this particular case, they seem to appear due to the inhibitory population, which tends to a periodic solution. What is more, the excitatory population presents a solution that oscillates close around the equilibrium.

6. CONCLUSIONS AND OPEN PROBLEMS

In this work, we have extended the results presented in [10–12] to the general NNLI self-contained mean-field model. This model is composed of two populations (excitatory and inhibitory), with transmission delays between the neurons, and where the neurons remain in a refractory state for a certain time. From an analytical point of view we have explored the number of steady states in terms of the model parameters (Thm. 3.1), the long time behaviour for small connectivity parameters (Thm. 3.3), and blow-up phenomena, if there is not a transmission delay between excitatory neurons (Thm. 3.5).

Besides analytical results, we have presented a numerical solver for this model (2.6), based on high order flux-splitting WENO schemes and an explicit third order TVD Runge-Kutta method, in order to describe

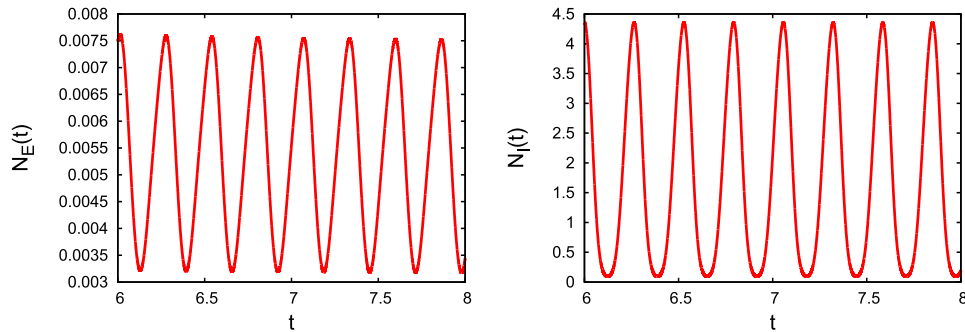


FIGURE 14. System (2.6) (two populations: excitatory and inhibitory) presents periodic solutions if there is a delay. We consider initial data (5.1) with $v_0^E = v_0^I = 1.25$ and $\sigma_0^E = \sigma_0^I = 0.0003$, $v_{\text{ext}} = 20$ and the connectivity parameters $b_E^E = 0.5$, $b_I^E = 0.75$, $b_I^I = 4$, $b_E^I = 1$ and with refractory states ($M_\alpha(t) = N_\alpha(t - \tau_\alpha)$) where $\tau_\alpha = 0.025$. The time evolution of the excitatory and inhibitory firing rates is showed.

the wide range of phenomena displayed by the network: Blow-up, asynchronous/synchronous solutions and instability/stability of the steady states. The solver also allows to observe the time evolution of not only the firing rates and refractory states, but also of the probability distributions of the excitatory and inhibitory populations. It was used to illustrate the result of Theorem 3.5: as long as the transmission delay of the excitatory to excitatory synapses is zero ($D_E^E = 0$), blow-up phenomena appear in the full NNLIIF model, even if there are nonzero transmission delays in the rest of the synapses. We remark that the numerical results suggest that blow-up phenomena disappear when the excitatory-to-excitatory transmission delay is nonzero, and the solutions may tend to a steady state or to a synchronous state or the firing rates increase without explosion in finite time. In the case of only one average-inhibitory population the behavior of the solutions after preventing a blow-up phenomenon seems to depend on the external firing rate v_{ext} . Furthermore, we have also observed periodic solutions for small values of the excitatory connectivity parameter combined with an initial data far from the threshold potential. Thus, synchronous solutions are not a direct consequence of having avoided the blow-up phenomenon.

Our numerical study is completed with the stability analysis of the steady states, when the network presents three of them. In our simulations, we do not observe bistability phenomena since the two upper stationary firing rates are unstable, while the lowest one is stable.

Finally, to our knowledge, the numerical solver presented in this paper is the first deterministic solver to describe the behavior of the full NNLIIF system involving all the characteristic phenomena of real networks. Including all relevant phenomena is essential to explore some open problems, as for instance: the analytical proof of the global existence of solution when there is a nonzero excitatory-to-excitatory transmission delay; the reasons why solutions tend to a steady state or to a synchronous state or the firing rates increase without blowing-up; and, an analytical study of the stability of the steady states when the connectivity parameters are not small.

Proving the existence of blow-up phenomena for the two populations model, when there is no delay between excitatory synapses, shows the importance of considering a nonzero excitatory-to-excitatory delay when the model is used to study the behavior of biological networks which do not synchronize [64]. On the other and, both the analytical and numerical results provided in this paper, can be interpreted from a biological point of view. For instance, the blow-up is usually related to a synchronization of a part of the network, while the number of steady states depending on the parameter values, might help to analyze situations of multi-stability for more complete NNLIIF models, as, e.g., conductance-based ones. In the literature, multi-stable networks are related to the visual perception and the decision making [3, 37], the short term working memory [79] and oculomotor integrators [44]. Also, the periodic or oscillatory solutions that we have observed numerically are

interesting, since they are used to model synchronous states and oscillations, observed, *e.g.*, during cortical processing [37, 40].

Acknowledgements. The authors acknowledge support from projects MTM2011-27739-C04-02 and MTM2014-52056-P of Spanish Ministerio de Economía y Competitividad and the European Regional Development Fund (ERDF/FEDER). The second author was also sponsored by the grant BES-2012-057704.

REFERENCES

- [1] L.F. Abbott and C. van Vreeswijk, Asynchronous states in networks of pulse-coupled oscillators. *Phys. Rev. E* **48** (1993) 1483–1490.
- [2] J. Acebrón, A. Bulsara and W.J. Rappel, Noisy Fitzhugh-Nagumo model: from single elements to globally coupled networks. *Phys. Rev. E* **69** (2004) 026202.
- [3] L. Albantakis and G. Deco, The encoding of alternatives in multiple-choice decision making. *Proc. Natl. Acad. Sci. USA* **106** (2009) 10308–10313.
- [4] F. Pfaftrre, C. Ly and D. Tranchina, Population density methods for stochastic neurons with realistic synaptic kinetics: firing rate dynamics and fast computational methods. *Netw. Comput. Neural Syst.* **17** (2006) 373–418.
- [5] G. Barna, T. Grobler and P. Erdi, Statistical model of the hippocampal CA3 region, II. The population framework: model of rhythmic activity in CA3 slice. *Biol. Cybern.* **79** (1998) 309–321.
- [6] R. Brette and W. Gerstner, Adaptive exponential integrate-and-fire model as an effective description of neural activity. *J. Neurophysiol.* **94** (2005) 3637–3642.
- [7] N. Brunel, Dynamics of sparsely connected networks of excitatory and inhibitory spiking networks. *J. Comput. Neurosci.* **8** (2000) 183–208.
- [8] N. Brunel and V. Hakim, Fast global oscillations in networks of integrate-and-fire neurons with long firing rates. *Neural Comput.* **11** (1999) 1621–1671.
- [9] N. Brunel and X.J. Wang, What determines the frequency of fast network oscillations with irregular neural discharge? I. Synaptic dynamics and excitation-inhibition balance. *J. Neurophysiol.* **90** (2003) 415–430.
- [10] M.J. Cáceres and B. Perthame, Beyond blow-up in excitatory integrate and fire neuronal networks: refractory period and spontaneous activity. *J. Theory Biol.* **350** (2014) 81–89.
- [11] M.J. Cáceres and R. Schneider, Blow-up, steady states and long time behaviour of excitatory-inhibitory nonlinear neuron models. *Kinet. Relat. Model.* **10** (2017) 587–612.
- [12] M.J. Cáceres, J.A. Carrillo and B. Perthame, Analysis of nonlinear noisy integrate & fire neuron models: blow-up and steady states. *J. Math. Neurosci.* **1** (2011) 7.
- [13] M.J. Cáceres, J.A. Carrillo and L. Tao, A numerical solver for a nonlinear Fokker-Planck equation representation of neuronal network dynamics. *J. Comput. Phys.* **230** (2011) 1084–1099.
- [14] D. Cai, L. Tao and D.W. McLaughlin, An embedded network approach for scale-up of fluctuation-driven systems with preservation of spike information. *PNAS* **101** (2004) 14288–14293.
- [15] D. Cai, L. Tao, M. Shelley and D.W. McLaughlin, An effective kinetic representation of fluctuation-driven neuronal networks with application to simple and complex cells in visual cortex. *Proc. Natl. Acad. Sci. USA* **101** (2004) 7757–7762.
- [16] J.A. Carrillo and F. Vecil, Nonoscillatory interpolation methods applied to Vlasov-based models. *SIAM J. Sci. Comput.* **29** (2007) 1179–1206.
- [17] J.A. Carrillo, I.M. Gamba, A. Majorana and C.-W. Shu, A WENO-solver for the transients of Boltzmann-Poisson system for semiconductor devices: performance and comparisons with Monte Carlo methods. *J. Comput. Phys.* **184** (2003) 498–525.
- [18] J.A. Carrillo, I.M. Gamba, A. Majorana and C.-W. Shu, 2D semiconductor device simulations by Weno-Boltzmann schemes: efficiency, boundary conditions and comparison to Monte Carlo methods. *J. Comput. Phys.* **214** (2006) 55–80.
- [19] J.A. Carrillo, M.d.M. González, M.P. Gualdani and M.E. Schonbek, Classical solutions for a nonlinear Fokker-Planck equation arising in computational neuroscience. *Commun. Partial Differ. Equ.* **38** (2013) 385–409.
- [20] J. Carrillo, B. Perthame, D. Salort and D. Smets, Qualitative properties of solutions for the noisy integrate & fire model in computational neuroscience. *Nonlinearity* **25** (2015) 3365–3388.
- [21] T. Chawanya, A. Aoyagi, T. Nishikawa, K. Okuda and Y. Kuramoto, A model for feature linking via collective oscillations in the primary visual cortex. *Biol. Cybern.* **68** (1993) 483–490.
- [22] J. Chevallier, Mean-Field Limit of Generalized Hawkes Processes. Preprint [arXiv:1510.05620](https://arxiv.org/abs/1510.05620) (2015).
- [23] J. Chevallier, M.J. Cáceres, M. Doumic and P. Reynaud-Bouret, Microscopic approach of a time elapsed neural model. *Math. Model. Methods Appl. Sci.* **25** (2015) 2669–2719.
- [24] F. Delarue, J. Inglis, S. Rubenthaler and E. Tanré, Global solvability of a networked integrate-and-fire model of McKean-Vlasov type. *Ann. Appl. Probab.* **25** (2015) 2096–2133.
- [25] F. Delarue, J. Inglis, S. Rubenthaler and E. Tanré, Particle systems with a singular mean-field self-excitation. Application to neuronal networks. *Stoch. Process. Appl.* **125** (2015) 2451–2492.
- [26] G. Dumont and P. Gabriel, The Mean-Field Equation of a Leaky Integrate-and-Fire Neural Network: Measure Solutions and Steady States. Preprint [arXiv:1710.05596](https://arxiv.org/abs/1710.05596) (2017).
- [27] G. Dumont and J. Henry, Population density models of integrate-and-fire neurons with jumps: well-posedness. *J. Math. Biol.* **67** (2012) 453–481.

- [28] G. Dumont and J. Henry, Synchronization of an excitatory integrate-and-fire neural network. *Bull. Math. Biol.* **75** (2013) 629–648.
- [29] G. Dumont, J. Henry and C.O. Tarniceriu, Noisy threshold in neuronal models: connections with the noisy leaky integrate-and-fire model. *J. Math. Biol.* **73** (2016) 1413–1436.
- [30] G. Dumont, J. Henry and C.O. Tarniceriu, Theoretical connections between mathematical neuronal models corresponding to different expressions of noise. *J. Theor. Biol.* **406** (2016) 31–41.
- [31] G. Dumont, J. Henry and C.O. Tarniceriu, A Theoretical Connection Between the Noisy Leaky Integrate-and-Fire and Escape Rate Models: The Non-Autonomous Case. Preprint [arXiv:1702.01391](https://arxiv.org/abs/1702.01391) (2017).
- [32] R. Fitzhugh, Impulses and physiological states in theoretical models of nerve membrane. *Biophys. J.* **1** (1961) 445–466.
- [33] N. Fourcaud and N. Brunel, Dynamics of the firing probability of noisy integrate-and-fire neurons. *Neural Comput.* **14** (2002) 2057–2110.
- [34] W. Gerstner, Population dynamics of spiking neurons: fast transients, asynchronous states, and locking. *Neural Comput.* **12** (2000) 43–89.
- [35] W. Gerstner, Integrate-and-fire neurons and networks, in *The Handbook of Brain Theory and Neural Networks*, Vol. 2. (2002) 577–581.
- [36] W. Gerstner and W. Kistler, *Spiking Neuron Models*. Cambridge University Press, Cambridge (2002).
- [37] C.M. Gray and W. Singer, Stimulus-specific neuronal oscillations in orientation columns of cat visual cortex. *Proc. Natl. Acad. Sci. USA* **86** (1989) 1698–1702.
- [38] T. Guillamon, An introduction to the mathematics of neural activity. *Bull. Soc. Catalana Mat.* **19** (2004) 25–45.
- [39] E. Haskell, D. Nykamp and D. Tranchina, Population density methods for large-scale modeling of neuronal networks with realistic synaptic kinetics: cutting the dimension down to size. *Netw. Comput. Neural Syst.* **12** (2001) 141–174.
- [40] J.A. Henrie and R. Shapley, LFP power spectra in V1 cortex: the graded effect of stimulus contrast. *J. Neurophysiol.* **94** (2005) 479–490.
- [41] E.M. Izhikevich and G.M. Edelman, Large-scale model of mammalian thalamocortical systems. *Proc. Natl. Acad. Sci. USA* **105** (2008) 3593–3598.
- [42] G.-S. Jiang and C.-W. Shu, Efficient implementation of weighted ENO schemes. *J. Comput. Phys.* **126** (1996) 202–228.
- [43] B. Knight, Dynamics of encoding in a population neurons. *J. Gen. Physiol.* **59** (1972) 734–766.
- [44] A. Koulakov, S. Raghavachari, A. Kepecs and J. Lisman, Model for a robust neural integrator. *Nat. Neurosci.* **5** (2002) 775–782.
- [45] R.J. LeVeque, *Numerical Methods for Conservation Laws*, 2nd edn. *Lectures in Mathematics*. Birkhäuser (1992).
- [46] J. Marino, J. Schummers, D.C. Lyon, L. Schwabe, O. Beck, P. Wiesing, et al., Invariant computations in local cortical networks with balanced excitation and inhibition. *Nat. Neurosci.* **8** (2005) 194–201.
- [47] M. Mattia and P. Del Giudice, Population dynamics of interacting spiking neurons. *Phys. Rev. E* **66** (2002) 051917.
- [48] S. Mischler, C. Quininao and J. Touboul, On a kinetic Fitzhugh–Nagumo model of neuronal network. *Commun. Math. Phys.* **342** (2016) 1001–1042.
- [49] K. Newhall, G. Kovačić, P. Kramer, A.V. Rangan and D. Cai, Cascade-induced synchrony in stochastically driven neuronal networks. *Phys. Rev. E* **82** (2010) 041903.
- [50] K. Newhall, G. Kovačić, P. Kramer, D. Zhou, A.V. Rangan and D. Cai, Dynamics of current-based, poisson driven, integrate-and-fire neuronal networks. *Commun. Math. Sci.* **8** (2010) 541–600.
- [51] D. Nykamp and D. Tranchina, A population density method that facilitates large-scale modeling of neural networks: analysis and application to orientation tuning. *J. Comput. Neurosci.* **8** (2000) 19–50.
- [52] D. Nykamp and D. Tranchina, A population density method that facilitates large-scale modeling of neural networks: Extension to slow inhibitory synapses. *Neural Comput.* **13** (2001) 511–546.
- [53] A. Omurtag, B.W. Knight and L. Sirovich, On the simulation of large populations of neurons. *J. Comput. Neurosci.* **8** (2000) 51–63.
- [54] K. Pakdaman, B. Perthame and D. Salort, Dynamics of a structured neuron population. *Nonlinearity* **23** (2010) 55–75.
- [55] K. Pakdaman, B. Perthame and D. Salort, Relaxation and self-sustained oscillations in the time elapsed neuron network model. *SIAM J. Appl. Math.* **73** (2013) 1260–1279.
- [56] K. Pakdaman, B. Perthame and D. Salort, Adaptation and fatigue model for neuron networks and large time asymptotics in a nonlinear fragmentation equation. *J. Math. Neurosci.* **4** (2014) 1–26.
- [57] B. Perthame and D. Salort, On a voltage-conductance kinetic system for integrate and fire neural networks. *Kinet. Relat. Model. AIMS* **6** (2013) 841–864.
- [58] A.V. Rangan and D. Cai, Fast numerical methods for simulating large-scale integrate-and-fire neuronal networks. *J. Comput. Neurosci.* **22** (2007) 81–100.
- [59] A.V. Rangan, D. Cai and D.W. McLaughlin, Modeling the spatiotemporal cortical activity associated with the line-motion illusion in primary visual cortex. *PNAS* **102** (2005) 18793–18800.
- [60] A.V. Rangan, D. Cai and D.W. McLaughlin, Quantifying neuronal network dynamics through coarse-grained event trees. *PNAS* **105** (2008) 10990–10995.
- [61] A.V. Rangan, G. Kovačić and D. Cai, Kinetic theory for neuronal networks with fast and slow excitatory conductances driven by the same spike train. *Phys. Rev. E* **77** (2008) 1–13.
- [62] A. Renart, N. Brunel and X.-J. Wang, Mean-field theory of irregularly spiking neuronal populations and working memory in recurrent cortical networks, in *Computational Neuroscience: A Comprehensive Approach*, edited by J. Feng. *CRC Mathematical Biology and Medicine Series*. Chapman & Hall (2004).

- [63] H. Risken, The Fokker-Planck Equation: Methods of Solution and Approximations, 2nd edn. Vol. 18 of *Springer Series in Synergetics*. Springer-Verlag, Berlin (1989).
- [64] P. Robert and J. Touboul, On the dynamics of random neuronal networks. *J. Stat. Phys.* **165** (2016) 545–584.
- [65] C. Rossant, D.F.M. Goodman, B. Fontaine, J. Platkiewicz, A.K. Magnusson and R. Brette, Fitting neuron models to spike trains. *Front. Neurosci.* **5** (2011) 1–8.
- [66] M. Shelley and L. Tao, Efficient and accurate time-stepping schemes for integrate-and-fire neuronal networks. *J. Comput. Neurosci.* **11** (2001) 111–119.
- [67] C.-W. Shu, Essentially non-oscillatory and weighted essentially non-oscillatory schemes for hyperbolic conservation laws, in *Advanced Numerical Approximation of Nonlinear Hyperbolic Equations*, Vol. 1697, edited by B. Cockburn, C. Johnson, C.-W. Shu, E. Tadmor and A. Quarteroni. Springer (1998) 325–432.
- [68] C.-W. Shu and S. Osher, Efficient implementation of essentially non-oscillatory shock-capturing schemes. *J. Comput. Phys.* **77** (1988) 439–471.
- [69] D.C. Somers, S.B. Nelson and M. Sur, An emergent model of orientation selectivity in cat visual cortical simple cells. *J. Neurosci.* **15** (1995) 5448–5465.
- [70] L. Tao, M. Shelley, D. McLaughlin and R. Shapley, An egalitarian network model for the emergence of simple and complex cells in visual cortex. *Proc. Natl. Acad. Sci. USA* **101** (2004) 366–371.
- [71] J. Touboul, Bifurcation analysis of a general class of nonlinear integrate-and-fire neurons. *SIAM J. Appl. Math.* **68** (2008) 1045–1079.
- [72] J. Touboul, Importance of the cutoff value in the quadratic adaptive integrate-and-fire model. *Neural Comput.* **21** (2009) 2114–2122.
- [73] J. Touboul, Limits and dynamics of stochastic neuronal networks with random heterogeneous delays. *J. Stat. Phys.* **149** (2012) 569–597.
- [74] J. Touboul, Propagation of chaos in neural fields. *Ann. Appl. Probab.* **24** (2014) 1298–1328.
- [75] J. Touboul, Spatially extended networks with singular multi-scale connectivity patterns. *J. Stat. Phys.* **156** (2014) 546–573.
- [76] A. Treves, Mean field analysis of neuronal spike dynamics. *Network* **4** (1993) 259–284.
- [77] T. Troyer, A. Krukowski, N. Priebe and K. Miller, Contrast invariant orientation tuning in cat visual cortex with feedforward tuning and correlation based intracortical connectivity. *J. Neurosci.* **18** (1998) 5908–5927.
- [78] H. Tuckwell, *Introduction to Theoretical Neurobiology*. Cambridge University Press, Cambridge (1988).
- [79] X. Wang, Synaptic basis of cortical persistent activity: the importance of NMDA receptors to working memory. *J. Neurosci.* **19** (1999) 9587–9603.
- [80] W. Wilbur and J. Rinzel, A theoretical basis for large coefficient of variation and bimodality in neuronal interspike interval distributions. *J. Theor. Biol.* **105** (1983) 345–368.